https://doi.org/10.5194/egusphere-2026-6788
Preprint. Discussion started: 17 November 2026
© Author(s) 2026. CC BY 4.0 License.

Uncertainty in Regional Monsoon Responses to Solar Radiation Modification Is Often Greater Across Models Than Across Strategies

Cindy Wang[1], Daniele Visioni[1], Brendan Clark[1], Zachary M. Labe[2], Bor-Ting Jong[3,4], Matthew Henry[5], Walker Lee[6], and Haruki Hirasawa[7]

[1]Department of Earth and Atmospheric Sciences, Cornell University, Ithaca, NY, USA
[2]Climate Central, Inc., Princeton, NJ, United States of America
[3]Department of Earth Sciences, Vrije Universiteit Amsterdam, Amsterdam, The Netherlands
[4]Institute for Environmental Studies, Vrije Universiteit Amsterdam, Amsterdam, The Netherlands
[5]Department of Mathematics, University of Exeter, UK
[6]Climate & Global Dynamics Division, National Science Foundation's National Center for Atmospheric Research (NSF NCAR), Boulder, CO, USA
[7]Department of Atmospheric and Climate Science, University of Washington, Seattle, WA, USA

Correspondence: Cindy Wang (cindywang@cornell.edu)

Abstract. Proposed solar radiation modification (SRM) strategies designed to stabilize global-mean surface temperature could alter regional monsoon systems. We examine changes in monsoon onset, retreat, duration, peak timing, active-season precipitation, wet-day frequency, and wet-day intensity across six monsoon regions in four Earth system models (CESM2, UKESM1, E3SMv3, and MIROC-ES2H). We compare projections under SSP2-4.5, a moderate greenhouse-gas emissions scenario, with three SRM strategies designed to keep global-mean surface temperature at 2020–2039 SSP2-4.5 mean (nominally 1.5°C above pre-industrial levels): stratospheric aerosol injection (SAI) at mid-latitudes, seasonal SAI at high latitudes, and marine cloud brightening (MCB) over mid-latitude oceans. Under SSP2-4.5, active-season precipitation increases in most monsoon regions, accompanied by delayed retreat and, in the East Asian and Australian–Maritime Continent monsoons, earlier onset and longer rainy seasons. Both SAI strategies reduce the magnitude of the late-century precipitation increases projected under SSP2-4.5. However, MCB retains larger positive precipitation anomalies than the SAI strategies in several regions, consistent with its distinct spatial forcing pattern and hydrological response. Monsoon duration is most often the leading contributor to active-season precipitation changes, while wet-day intensity plays a more model-dependent secondary role. Overall, differences among models exceed differences between SRM strategies in most region–metric combinations. The South Asian monsoon is a notable exception: differences among SRM strategies exceed intermodel differences for most monsoon metrics, indicating that outcomes in this region are particularly sensitive to the choice of SRM intervention. These results underscore the importance of multi-model ensembles for evaluating regional SRM impacts, as conclusions based on individual models may overstate or obscure differences among simulated intervention strategies.

https://doi.org/10.5194/egusphere-2026-6788
Preprint. Discussion started: 17 November 2026
© Author(s) 2026. CC BY 4.0 License.

1 Introduction

Solar radiation modification (SRM) has been proposed as a potential approach to reduce some of the impacts of anthropogenic warming by decreasing absorbed solar radiation. Two widely discussed SRM strategies are stratospheric aerosol injection (SAI), in which aerosols or aerosol precursors are introduced into the stratosphere to increase planetary albedo, and marine cloud brightening (MCB), in which sea salt aerosols (SSA) are used to brighten low marine clouds, thereby increasing their reflectivity. Because both strategies can reduce global-mean surface air temperature (GMSAT), SRM experiments are often designed around maintaining a consistent temperature target, such as limiting global warming to 1.5°C above the 1850–1900 pre-industrial mean. However, restoring GMSAT to a reference target does not necessarily restore regional climate conditions, particularly those associated with the hydrological cycle (Tilmes et al., 2013; Haywood et al., 2023; Lee et al., 2025a; Wang et al., 2026b).

Precipitation responses are shaped not only by thermodynamic changes in global mean temperature, but also by changes in atmospheric circulation, moisture transport, energetic constraints, aerosols, and the spatial and seasonal distribution of radiative forcing. These controls can respond differently under greenhouse-gas forcing, SAI, and MCB. As a result, even when SRM returns global or regional temperature toward a baseline target, regional precipitation may not simply retrace the greenhouse-gas-driven response, but instead shift toward a distinct hydroclimate state that differs from both the target and the background climate.

Monsoon regions are particularly important in this context because their seasonal rainfall supports large populations, agricultural systems, ecosystems, and water resources (Webster et al., 1998; Gadgil and Gadgil, 2006; Wang, 2006; Turner and Annamalai, 2012; IPCC, 2021). Agricultural calendars in many monsoon regions are closely synchronized with the onset and retreat of the rainy season (e.g., the *kharif* season in South Asia, rainy-season millet and sorghum cultivation in the Sahel, and rice production across East and Southeast Asia), so shifts in monsoon timing can shorten the growing season or disrupt harvest. How rainfall is distributed throughout the season also matters: for the same seasonal total, rainfall delivered through frequent moderate events can have very different consequences for soil moisture, runoff, and ecosystem or crop productivity than rainfall delivered through a few intense events (Knapp et al., 2008; Bronstert et al., 2023).

Modeling studies have previously identified changes in monsoon characteristics from SRM. Robock et al. (2008) found that both tropical and Arctic stratospheric sulfur dioxide (SO_2) injection disrupted the Asian and African summer monsoons and reduced precipitation. Bonou et al. (2023) also found substantial reductions in Sahelian monsoon precipitation under SAI, linked primarily to weakened monsoon circulation and shifts in the spatial distribution of rainfall. For MCB, Odoulami et al. (2024) found mixed Sahelian responses to subtropical MCB, depending on the deployment location. These results established monsoon weakening and regional drought as potential consequences of SRM, concerns subsequently highlighted in broader assessments of SAI risks (Robock et al., 2009) and reinforced by more recent studies of global and regional monsoon responses (Sun et al., 2020; Asutosh et al., 2025). In a 12-model Geoengineering Model Intercomparison Project (GeoMIP) analysis, Tilmes et al. (2013) found that idealized SRM weakened the global hydrological cycle and produced robust reductions in monsoonal land precipitation in several regions.

https://doi.org/10.5194/egusphere-2026-6788
Preprint. Discussion started: 17 November 2026
© Author(s) 2026. CC BY 4.0 License.

Many of these results also come from idealized designs. In GeoMIP G1, an abrupt quadrupling of CO_2 is offset by an equally abrupt reduction in the solar constant, and monsoon precipitation decreases in most regions (Tilmes et al., 2013). Singh et al. (2026) balanced a doubling of CO_2 with a globally uniform stratospheric sulfate layer, finding that SAI partially revives the Indian monsoon circulation and low-pressure-system activity but reduces Indian summer rainfall and its extremes. Robock et al. (2008) imposed constant SO_2 injection rates from the start of the simulation, producing an abrupt, fixed cooling rather than one that responds to the warming it offsets. These idealized experiments have further demonstrated that the spatial distribution of aerosol forcing, including its latitudinal placement and hemispheric asymmetry, can strongly influence monsoon rainfall. Krishnamohan and Bala (2022) showed that monsoon precipitation generally decreases in the hemisphere in which aerosols are preferentially injected and increases in the opposite hemisphere, through changes in the interhemispheric temperature gradient and displacement of the Intertropical Convergence Zone (ITCZ). Roose et al. (2023) subsequently quantified this relationship, linking interhemispheric differences in stratospheric aerosol optical depth and radiative forcing to shifts in the ITCZ and tropical monsoon precipitation.

Existing studies of SRM impacts on monsoons have often focused on a single monsoon region, climate model, or intervention strategy. This makes it difficult to determine whether differences in projected monsoon responses arise primarily from structural differences among climate models, internal variability, or the choice of intervention strategy. Addressing this uncertainty requires coordinated comparisons across both models and SRM strategies.

A second gap concerns how SRM affects the seasonal characteristics of monsoon rainfall. Relatively little attention has been given to how SRM alters monsoon timing (onset, retreat, duration, and peak timing) and the distribution of rainfall within the season (wet-day frequency and rainfall intensity). Recent work has begun to address this question for the South American monsoon, finding that SAI can largely preserve historical monsoon timing and duration while precipitation intensity remains altered (Gabriel et al., 2026). This distinction is important because annual or seasonal rainfall totals may change little even when the timing, persistence, or intensity of the rainy season changes substantially.

Monsoon circulation responses to SRM depend not only on the latitude and hemispheric asymmetry of the forcing, but also on how the forcing is produced and distributed spatially. Different SRM strategies may therefore produce distinct regional monsoon responses despite achieving similar global cooling. SAI and MCB both reduce absorbed solar radiation, but through different physical mechanisms and spatial forcing patterns. SAI increases stratospheric aerosol loading, producing a relatively broad shortwave forcing while also modifying stratospheric heating, meridional temperature gradients, large-scale circulation, and tropical precipitation patterns (Rasch et al., 2008; Tilmes et al., 2013; Kravitz et al., 2013; Niemeier and Tilmes, 2017; Visioni et al., 2021). In contrast, MCB acts within the lower troposphere by increasing cloud condensation nuclei over marine low-cloud regions, enhancing cloud droplet number concentration and cloud albedo through aerosol–cloud interactions (Latham et al., 2008; Jones et al., 2009; Bala et al., 2011; Stjern et al., 2018). Because MCB forcing is tied to the location and frequency of marine boundary-layer clouds, its forcing and resulting circulation response can be more spatially heterogeneous and sensitive to regional cloud and surface-flux changes (Alterskjær and Kristjánsson, 2013; Hill and Ming, 2012; Baughman et al., 2012; Stjern et al., 2018; Hirasawa et al., 2026a; Wang et al., 2026a).

https://doi.org/10.5194/egusphere-2026-6788
Preprint. Discussion started: 17 November 2026
© Author(s) 2026. CC BY 4.0 License.

Together, these considerations motivate a systematic assessment of whether monsoon responses are robust across climate models and SRM strategies, and whether those responses emerge through changes in seasonal timing and rainfall distribution that may not be apparent from seasonal totals alone. We assess how regional monsoons respond to SRM under a temperature-stabilization pathway rather than an idealized forcing. We compare changes in monsoon onset, retreat, duration, peak timing, active-season precipitation, wet-day frequency, and wet-day intensity across six monsoon regions, four climate models, and three SRM strategies. We ask (1) how effectively SRM restores regional monsoon characteristics toward the 2020–2039 SSP2-4.5 reference climate, (2) whether residual precipitation changes arise primarily from changes in monsoon timing, frequency, or intensity, and (3) whether regional responses differ more across climate models or across SRM strategies.

2 Methodology

2.1 SRM experiments and model configurations

All SRM strategies are deployed under the moderate emissions scenario SSP2-4.5 (O'Neill et al., 2016) beginning in 2035, and are designed to keep GMSAT at each model's own 2020–2039 SSP2-4.5 mean. This target is nominally 1.5°C above pre-industrial levels. A summary of all experiments, ensemble sizes, and analysis periods is provided in Table 1. The primary analysis focuses on changes in monsoon characteristics between a reference period (2020–2039) and a future period (2065–2084) under SSP2-4.5, G6-1.5K-SAI, G6-1.5K-HiLLA, and G6-1.5K-MCB (Visioni et al., 2026).

Four Earth system models (ESMs) participated in these experiments: the Community Earth System Model version 2 (CESM2; Danabasoglu et al. (2020)), the UK Earth System Model (UKESM1; Sellar et al. (2019)), the Energy Exascale Earth System Model (E3SM; Golaz et al. (2026)), and the Model for Interdisciplinary Research on Climate (MIROC-ES2H, hereafter MIROC; Kawamiya et al. (2020)). The participating model configurations of CESM2 and E3SM are not identical across all experiments. The historical, SSP2-4.5, G6-1.5K-SAI, and G6-1.5K-HiLLA simulations use CESM2 with the Whole Atmosphere Community Climate Model version 6 (WACCM6; Gettelman et al. (2019)) and E3SMv3, whereas the G6-1.5K-MCB simulations were performed with CESM2.1-CAM6 and E3SMv2. These configurations differ: CESM2(WACCM6) and CESM2.1-CAM6 differ in stratospheric vertical resolution and chemistry, and E3SMv2 and E3SMv3 differ in aerosol and cloud parameterizations and in mean-state biases (Golaz et al., 2022). Consequently, for CESM2 and E3SM, the contrast between G6-1.5K-MCB and the two SAI experiments confounds the intervention with the underlying model version. All UKESM1 simulations use UKESM1.1, but the SSP2-4.5 control for G6-1.5K-SAI and G6-1.5K-HiLLA includes heterogeneous chemistry on stratospheric aerosols, whereas the SSP2-4.5 control for G6-1.5K-MCB does not; the two sets of UKESM1 control members are independent and not paired (Mulcahy et al., 2023).

We therefore do not interpret differences between MCB and SAI in these models as arising solely from the intervention strategy; instead, we emphasize responses that are consistent across models and treat model-version differences as an additional source of structural uncertainty. We retain explicit version labels in Table 1; for brevity, we refer to the models as CESM2, UKESM1, E3SM, and MIROC hereafter. To test whether differences between MCB and SAI reflect the intervention or the

https://doi.org/10.5194/egusphere-2026-6788
Preprint. Discussion started: 17 November 2026
© Author(s) 2026. CC BY 4.0 License.

model version, we repeat the model-versus-strategy comparison using only UKESM1 and MIROC, whose configurations are identical across the SAI and MCB experiments (Table S5).

Experiment	Description	Analysis Period	Model	Ensemble members
Historical	Observed CMIP6 historical forcing (greenhouse gases, aerosols, etc.)	1998–2014	CESM2(WACCM6)	3
			UKESM1-1-LL	3
			E3SMv3	3
			MIROC-ES2H	2
SSP2-4.5	Moderate emissions scenario (∼4.5 W m^{-2} by 2100; baseline for SAI experiments)	2020–2039 & 2065–2084	CESM2(WACCM6)	3
			UKESM1-1-LL	3
			E3SMv3	3
			MIROC-ES2H	10
G6-1.5K-SAI	SAI simulation with symmetric injections in two locations (30°N and 30°S)	2065–2084	CESM2(WACCM6)	3
			UKESM1-1-LL	3
			E3SMv3	3
			MIROC-ES2H	10
G6-1.5K-HiLLA	SAI simulations with seasonal injections for 4 months (March–June) at 60°N and 4 months (Sep–Dec) at 60°S at 15 km	2065–2084	CESM2(WACCM6)	3
			UKESM1-1-LL	3
			E3SMv3	3
			MIROC-ES2H	10
G6-1.5K-MCB	Increasing SSA emissions over five mid-latitude ocean regions	2065–2084	CESM2.1-CAM6	3
			UKESM1-1-LL	3
			E3SMv2	3
			MIROC-ES2H	10

Table 1. Summary of the experiments analyzed in this study, including injection configurations, participating models and model versions, ensemble sizes, and analysis periods. All changes are computed relative to the 2020–2039 mean of the corresponding SSP2-4.5 control simulation (the reference period).

The G6-1.5K-SAI experiment targets a restoration of GMSAT to 1.5°C above pre-industrial levels via symmetric SO_2 injections at 30°N and 30°S at approximately 21 km altitude (Lee et al., 2026; Visioni et al., 2024). The High-Latitude Low-Altitude Stratospheric Aerosol Injection experiment (G6-1.5K-HiLLA) pursues the same GMSAT target through a seasonally varying high-latitude strategy (Duffey et al., 2026), with injections at 60°N from March–June and at 60°S from September–December at ∼15 km altitude. Both SAI strategies are compared with the corresponding SSP2-4.5 future, which represents the corresponding future without SAI. All four models (CESM2, UKESM1, E3SMv3, and MIROC) contribute ensemble members to both SAI experiments, with the same member counts as listed above.

https://doi.org/10.5194/egusphere-2026-6788
Preprint. Discussion started: 17 November 2026
© Author(s) 2026. CC BY 4.0 License.

The G6-1.5K-MCB experiment pursues the same GMSAT target. In this experiment, idealized SSA emissions are applied over five mid-latitude ocean regions: the North Atlantic, North Pacific, South Atlantic, South Pacific, and South Indian oceans (as described in Hirasawa et al. (2026a, b); Chen et al. (2024)). These regions were selected so that midlatitude MCB produces a cooling pattern similar to that of G6-1.5K-SAI, which also more closely offsets the greenhouse-gas warming pattern than previously explored subtropical or tropical MCB strategies (Hirasawa et al., 2026b). The SSA emission rate is adjusted to maintain GMSAT near the 2020–2039 reference-period target, providing an MCB analogue to the GMSAT-controlled G6-1.5K-SAI and G6-1.5K-HiLLA experiments. The G6-1.5K-MCB simulations analyzed here were performed with CESM2.1-CAM6, E3SMv2, MIROC and UKESM1. Because the G6-1.5K-MCB simulations use different model versions or ensembles from the SAI simulations, each is compared with the SSP2-4.5 control run performed alongside it.

Throughout the paper, "SSP2-4.5" refers to the control simulations of the SAI experiments: CESM2(WACCM6), UKESM1-1-LL, E3SMv3 and MIROC-ES2H (Table 1). These are the simulations shown as SSP2-4.5 in Figs. 1, 3 and 4 and in Table S1, and they are the baseline for the G6-1.5K-SAI changes and, for CESM2 and UKESM1, for the G6-1.5K-HiLLA changes. G6-1.5K-MCB changes are always computed relative to the MCB control, SSP2-4.5-M (CESM2.1-CAM6 with 16 members, UKESM1-1-LL, E3SMv2 and MIROC-ES2H), and G6-1.5K-HiLLA changes in E3SM and MIROC relative to SSP2-4.5-H. For CESM2 and E3SM, the SSP2-4.5 and the SSP2-4.5-M therefore differ in model version as well as in ensemble, so a direct visual comparison of the SSP2-4.5 and G6-1.5K-MCB results (e.g., Fig. 1b and e) combines the effect of MCB with that of the model version.

Fig. S1 compares the two SSP2-4.5 versions directly. Their 2020–2039 monsoon-season precipitation differs significantly in about 40% of monsoon grid cells, whereas the difference between their projected 2065–2084 changes is smaller and significant in about one-third of grid cells (Fig. S1c, d). We therefore assess each SRM strategy only relative to its own control, interpret differences between G6-1.5K-MCB and the SAI strategies in CESM2 and E3SM with caution, and use UKESM1 and MIROC, whose configurations are the same across experiments, as a check (Table S4).

2.2 GPM IMERG precipitation

We use precipitation estimates from NASA's Global Precipitation Measurement (GPM) Integrated Multi-satellitE Retrievals for GPM (IMERG) Final Run product as an observational reference for evaluating historical monsoon characteristics (Huffman et al., 2023b, a). IMERG Final Run provides gridded global multi-satellite precipitation estimates at 30-minute temporal and $0.1^\circ \times 0.1^\circ$ spatial resolution. The product combines passive-microwave precipitation retrievals with microwave-calibrated infrared estimates using quasi-Lagrangian time interpolation, and incorporates gauge observations and climatological adjustments to improve precipitation estimates.

This observational product has been used as an observational benchmark for evaluating climate model precipitation in monsoon regions in several prior studies (Huang et al., 2021; Prakash et al., 2018; Zhang et al., 2025). Its demonstrated skill in representing mean monsoon rainfall and its variability across diverse regional settings (Prakash et al., 2018) makes it a reliable reference for assessing the large-scale monsoon characteristics simulated by the historical runs of CESM2, UKESM1, E3SM, and MIROC.

https://doi.org/10.5194/egusphere-2026-6788
Preprint. Discussion started: 17 November 2026
© Author(s) 2026. CC BY 4.0 License.

Daily IMERG precipitation over 1998–2014 and the historical simulations were analyzed over the same six monsoon domains. Because IMERG begins in January 1998 and the SAmerM and AusMCM monsoon year begins in October, the first complete monsoon year in these two regions is 1999; for SAmerM and AusMCM, both IMERG and the models therefore use 1999–2014. We use these estimates to characterize observed monsoon timing and rainfall properties and to quantify historical model biases. Historical biases are computed as the ensemble-mean model value minus the IMERG value for each region and metric. Where biases are compared with projected changes, both are expressed in physical units: days for onset, retreat, peak timing and duration, and percent for active-season precipitation and wet-day intensity (biases relative to the IMERG value, changes relative to each model's baseline). These comparisons provide context for assessing whether intermodel differences in projected SRM responses are associated with differences in historical monsoon representation.

2.3 Monsoon regions

The six monsoon regions and their primary monsoon seasons are defined in IPCC AR6 Chapter 8 (Section 8.3.2.4, Fig. 8.11; Douville et al. (2021)): (1) North American monsoon (NAmerM), July–September; (2) West African monsoon (WAfriM), June–September; (3) South Asian monsoon (SAsiaM), June–September; (4) East Asian monsoon (EAsiaM), June–August; (5) South American monsoon (SAmerM), December–February; and (6) Australian–Maritime Continent monsoon (AusMCM), December–February. These region- and season-specific definitions were used to calculate the monsoon-season precipitation totals shown in Fig. 1. Fig. 1a presents the multi-model SSP2-4.5 baseline climatology for 2020–2039, while Fig. 1b–e shows the corresponding 20-year mean precipitation changes relative to the 2020–2039 baseline of each experiment's own control: SSP2-4.5 for panels b–d (SSP2-4.5-H for G6-1.5K-HiLLA in E3SM and MIROC) and SSP2-4.5-M for panel e (Sect. 2.1; Fig. S1).

2.4 Calculating monsoon indices

Monsoon characteristics were evaluated over the six Intergovernmental Panel on Climate Change (IPCC) Sixth Assessment Report (AR6) monsoon regions (Iturbide et al., 2020) using precipitation from each model, simulation, ensemble member, and observational dataset. Daily precipitation was first aggregated into non-overlapping 5-day pentads, yielding 73 pentads per year (Feb 29 is omitted; for the 360-day UKESM1 calendar, the 72 pentads are padded to 73 by repeating the last pentad so that all models use the same pentad grid). The regional pentad precipitation time series was then used for all monsoon timing diagnostics and for the calculation of seasonal precipitation metrics. Monsoon onset and retreat were diagnosed from the regional pentad precipitation time series using a threshold-based method following the Wang and LinHo (2002) framework. Wang and LinHo (2002) developed a rainfall-based framework for diagnosing monsoon domains, onset, and withdrawal from pentad precipitation. They applied the method to the Asian-Pacific monsoon using pentad anomalies constructed with 12 Fourier harmonics and a fixed rainfall threshold; Zhang (2008) later extended the framework globally. Table 2 shows the monsoon metrics analyzed in this study. For each ensemble member and analysis period, the climatological pentad cycle was reconstructed from the period-mean pentad precipitation cycle using the first 12 Fourier harmonics. Onset, retreat, duration, and peak timing were diagnosed from this smoothed climatological cycle.

https://doi.org/10.5194/egusphere-2026-6788
Preprint. Discussion started: 17 November 2026
© Author(s) 2026. CC BY 4.0 License.

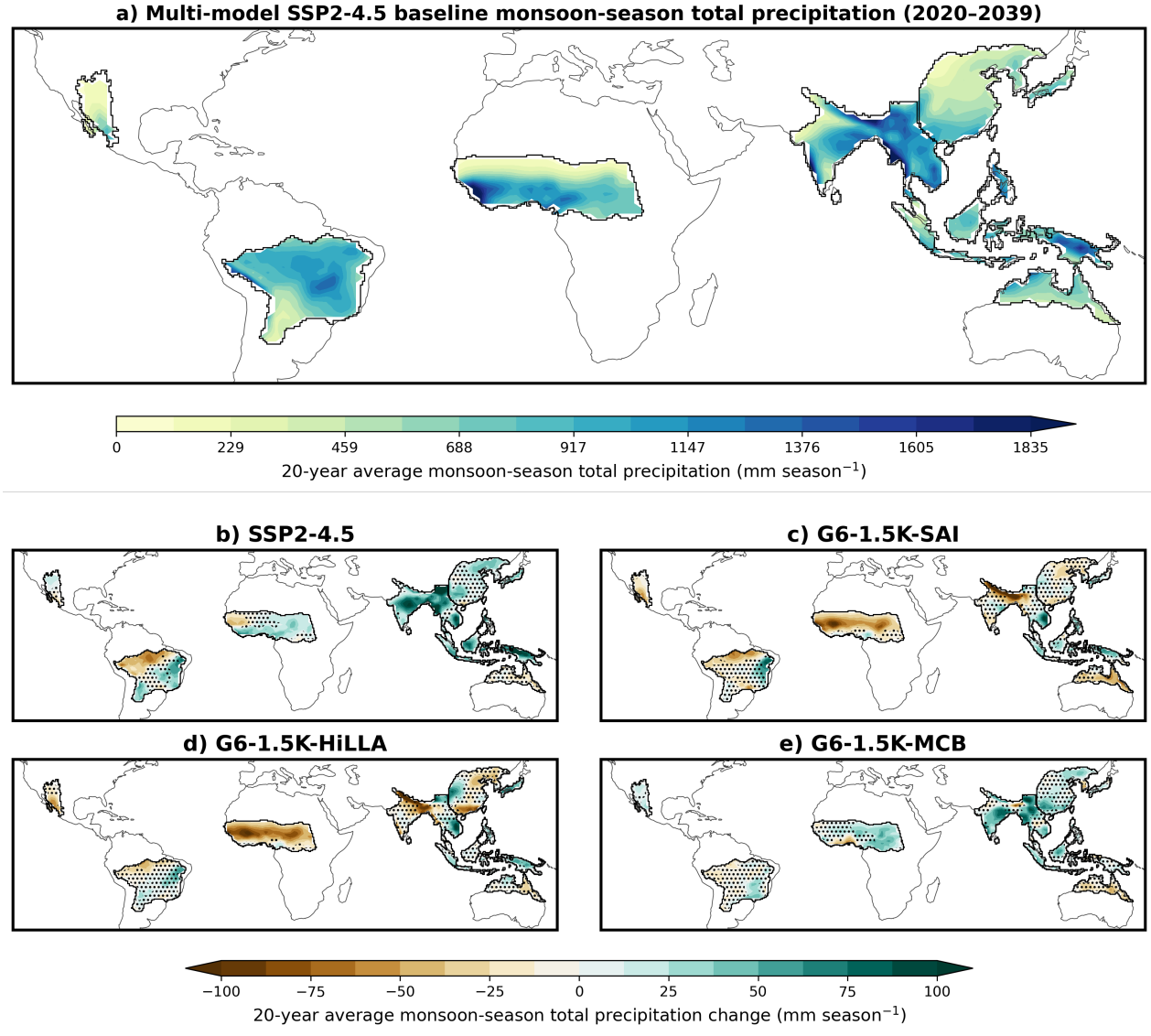


Figure 1. Multi-model mean monsoon-season total precipitation and projected changes across the major global monsoon regions. (a) SSP2-4.5 baseline monsoon-season total precipitation averaged over the reference period (2020–2039). (b–e) Twenty-year mean (2065–2084) changes in monsoon-season total precipitation relative to the corresponding SSP2-4.5 reference simulations (2020–2039) under (b) SSP2-4.5, (c) G6-1.5K-SAI, (d) G6-1.5K-HiLLA, and (e) G6-1.5K-MCB. Each experiment is compared against its matched SSP2-4.5 baseline ensemble. Stippling indicates changes that are not statistically significant at the 95% confidence level. Relative changes (%) are shown in Fig. S2.

To reduce sensitivity to short-lived precipitation anomalies, monsoon onset is defined as the first pentad of a period of at least two consecutive pentads with precipitation at or above the regional threshold that contains the seasonal precipitation maximum.

https://doi.org/10.5194/egusphere-2026-6788
Preprint. Discussion started: 17 November 2026
© Author(s) 2026. CC BY 4.0 License.

Metric	Definition	Change reported as
Onset	First pentad of the period of at least two consecutive pentads in which regional mean pentad precipitation is at or above the regional threshold and which contains the seasonal maximum.	days
Retreat	First pentad after the seasonal precipitation maximum at which regional mean pentad precipitation falls below the regional threshold and remains below it for two consecutive pentads.	days
Duration	Length of the active monsoon season, defined as the number of days from the first day of the onset pentad to the last day of the retreat pentad.	days
Peak timing	Pentad of maximum regional precipitation within the monsoon season.	days
Active-season precipitation	Total precipitation accumulated from the onset pentad through the retreat pentad (mm).	% of baseline
Wet-day frequency	Fraction of days with precipitation ≥ 1 mm day^{-1} during the active monsoon season.	% of baseline
Wet-day intensity	Mean daily precipitation on wet days during the active monsoon season (mm day^{-1}).	% of baseline

Table 2. Definitions of the monsoon metrics analyzed in this study. All metrics are computed from the regional, area-weighted mean daily precipitation within each IPCC monsoon domain, separately for each model, ensemble member, and scenario. Onset, retreat, peak timing, and duration are diagnosed once per member and period from the climatological pentad precipitation cycle, reconstructed as the period-mean pentad cycle plus its first 12 Fourier harmonics. Onset and retreat are diagnosed within region-specific analysis windows that extend beyond the core monsoon seasons: May–October for NAmerM; April–November for WAfriM and SAsiaM; April–October for EAsiaM; and October–April for SAmerM and AusMCM. Peak timing is the pentad of maximum precipitation between onset and retreat. Active-season precipitation, wet-day frequency, and wet-day intensity are computed for each monsoon year and then averaged over the 20-year period. All three metrics are evaluated over the diagnosed active monsoon season, from the onset pentad through the retreat pentad. Changes are computed between the 2020–2039 reference period of each experiment's control simulation and the 2065–2084 future period (Sect. 2.1).

A two-pentad persistence criterion, corresponding to at least 10 days of sustained above-threshold precipitation, has also been used to identify persistent rainy-season onset in previous pentad-based studies (LinHo et al., 2008). We adopt this criterion as a balance between excluding isolated threshold exceedances and avoiding a more restrictive persistence requirement that could delay the diagnosed onset across regions with differing monsoon climatologies. The additional requirement that the qualifying period contain the seasonal precipitation maximum further ensures that the diagnosed onset corresponds to the principal monsoon rainy season. Following the use of fixed absolute precipitation thresholds in previous regional onset studies (Janowiak and Xie, 2003; Nakaegawa et al., 2015; Seregina et al., 2019), we apply a region-specific but model- and scenario-invariant threshold to the domain-mean precipitation time series.

https://doi.org/10.5194/egusphere-2026-6788
Preprint. Discussion started: 17 November 2026
© Author(s) 2026. CC BY 4.0 License.

Within the same analysis window, retreat is the first pentad after the seasonal precipitation maximum at which precipitation falls below the threshold and remains below it for two consecutive pentads. This ensures that the seasonal peak lies within the diagnosed monsoon season and avoids spurious onsets from brief threshold exceedance outside the main rainy season. Monsoon duration was defined as the number of days from the first day of the onset pentad through the last day of the retreat pentad. Active-season precipitation was calculated for each year as the sum of daily precipitation from the first day of the onset pentad to the last day of the retreat pentad, using the active season diagnosed from the member's climatology for that period. Peak monsoon timing was defined as the pentad within the monsoon season with the maximum Fourier-reconstructed climatological precipitation.

The precipitation thresholds used to identify monsoon onset and retreat were 2.5 mm day^{-1} for the North American monsoon; 5 mm day^{-1} for the WAfrM, SAsiaM, EAsiaM, and SAmerM; and 7.5 mm day^{-1} for the AusMCM. While some studies have applied a single uniform threshold across all monsoon regions (Janowiak and Xie, 2003; Wang and LinHo, 2002), the thresholds adopted here are region-specific, chosen to be consistent with values reported in the literature for each monsoon system individually (Muñoz-Sanchez et al., 2024; Zhang, 2008; Evans et al., 2014) and to align with the climatological monsoon precipitation signal apparent in each region (Fig. 2; see Fig. S3 for individual models). Each region's threshold is held fixed across all models, ensemble members, periods, and scenarios.

Changes in active-season precipitation were decomposed into contributions from active-season duration D (days), wet-day frequency f, and wet-day intensity I (mm day^{-1}) using a logarithmic decomposition. Writing $L = \ln(P_{\mathrm{fut}}/P_{\mathrm{base}})$ for the log change in active-season precipitation between the future and reference periods, we use the following equation:

$$L = \ln\frac{D_{\mathrm{fut}}}{D_{\mathrm{base}}} + \ln\frac{f_{\mathrm{fut}}}{f_{\mathrm{base}}} + \ln\frac{I_{\mathrm{fut}}}{I_{\mathrm{base}}} + R \tag{1}$$

where all quantities are ensemble means and R is a residual. R measures the extent to which the identity $P = DfI$ fails to hold for the metrics as defined. In Fig. 5, each term in Eq. (1) is converted to percent-of-baseline units by multiplying by the factor $100\,(e^{L} - 1)/L$, so that the four plotted contributions sum exactly to the total percent change in active-season precipitation. Although P, D, f, and I are evaluated over the same diagnosed active-season interval, $P = DfI$ is not an exact identity for the period-mean metrics. The residual captures effects including precipitation on days below the 1 mm day^{-1} wet-day threshold and covariance introduced by averaging frequency and intensity separately across years and ensemble members.

2.5 Statistical testing

Uncertainty in each change was estimated with a hierarchical bootstrap (5000 resamples). In each resample, ensemble members were drawn with replacement and, within each drawn member, years were drawn with replacement; the member's climatological pentad cycle, timing metrics and active-season window were then recomputed from the resampled years, and per-year metrics were averaged over them. Baseline and future periods were resampled independently. Changes are considered significant when the 95% bootstrap confidence interval excludes zero. The reported change is the difference of ensemble means; the reported uncertainty is the standard deviation of the bootstrap distribution. For the spatial precipitation maps in Fig. 1, signifi-

https://doi.org/10.5194/egusphere-2026-6788
Preprint. Discussion started: 17 November 2026
© Author(s) 2026. CC BY 4.0 License.

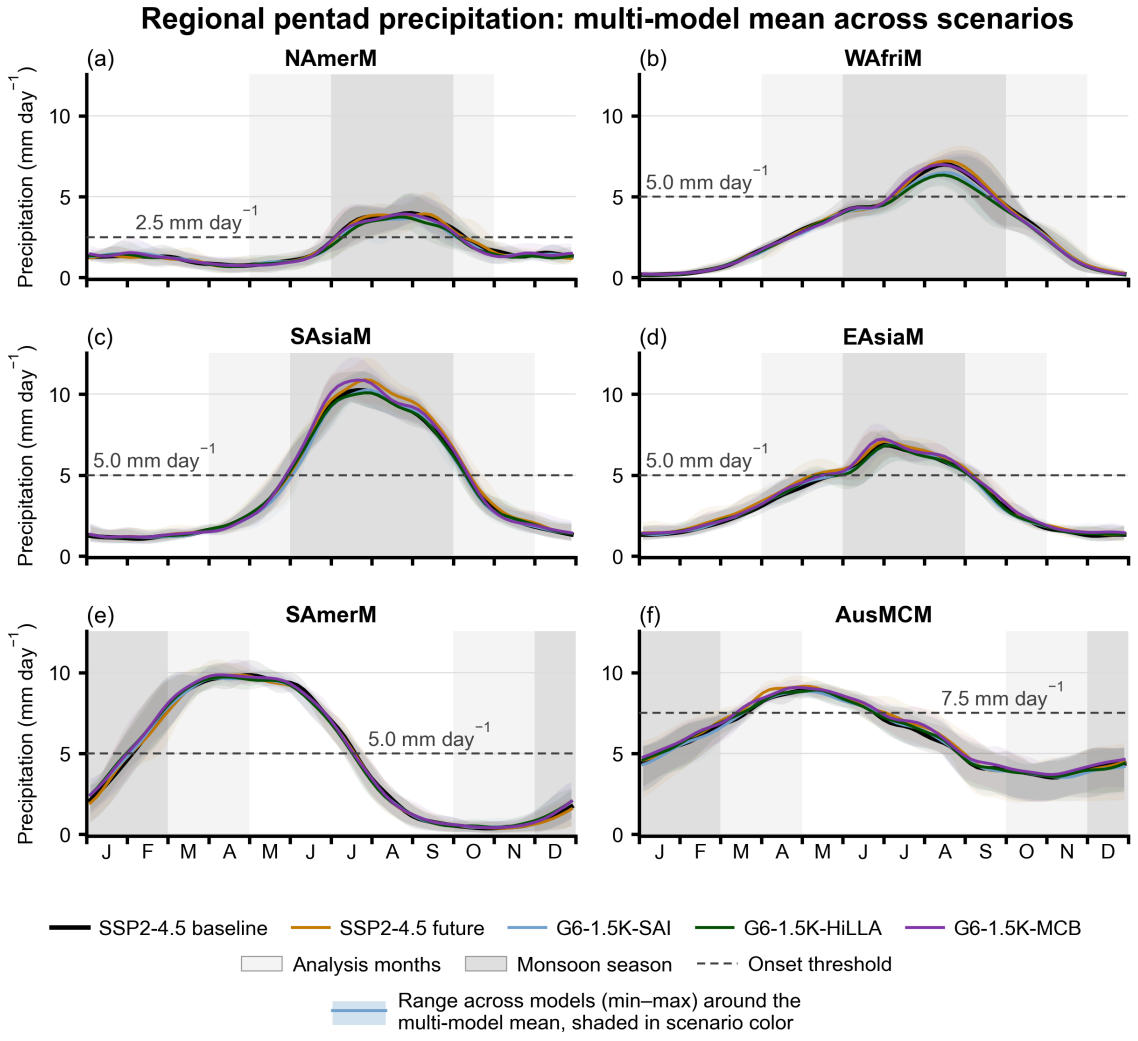


Figure 2. Multi-model mean regional pentad precipitation climatologies for six monsoon regions under SSP2-4.5 and SRM scenarios: (a) NAmerM, (b) WAfriM, (c) SAsiaM, (d) EAsiaM, (e) SAmerM, and (f) AusMCM. Curves show the ensemble-mean climatological pentad precipitation reconstructed using the mean seasonal cycle plus the first 12 Fourier harmonics for the SSP2-4.5 baseline (black), SSP2-4.5 future (orange), G6-1.5K-SAI (light blue), G6-1.5K-HiLLA (dark green), and G6-1.5K-MCB (purple). Dark gray shading marks the core monsoon season months used for each region, and light gray shading marks the extended monsoon period used in the analysis. Horizontal dashed line indicates the fixed onset threshold used in the monsoon timing analysis. Colored bands show the range across models (minimum to maximum) around each multi-model mean.

cance is assessed separately using a two-sided Welch t-test on member-years; significance for the regional monsoon metrics is assessed using the hierarchical bootstrap described above.

https://doi.org/10.5194/egusphere-2026-6788
Preprint. Discussion started: 17 November 2026
© Author(s) 2026. CC BY 4.0 License.

3 Results

3.1 Changes in monsoon onset, retreat, and active-season precipitation

To assess how regional monsoon characteristics respond across models and SRM intervention strategies, we compare changes in onset, retreat (days), and active-season precipitation (%) relative to the 2020–2039 SSP2-4.5 reference period in Fig. 3. Other monsoon metrics (duration change, peak timing change, and wet-day intensity change) are shown in Fig. S4.

Across the models, active-season precipitation generally increases under SSP2-4.5 in several monsoon regions (Fig. 3 right column; Table S1), consistent with assessments across several CMIP-generations showing an overall intensification of land monsoon precipitation under greenhouse-gas warming, particularly across the Asian and African monsoon regions (Wang et al., 2014; Jin et al., 2020). NAmerM is a notable exception to this broader tendency and exhibits intermodel disagreement in our simulations, with CESM2 showing a markedly different response from the other models (-35% versus +7 to +10%; Fig. 3c, f, i, and l), large enough to make the multi-model mean change slightly negative (-1.8%; Table S1). This large model dependence also reflects the substantial uncertainty documented in the magnitude and seasonality of projected NAmerM rainfall, including a tendency toward reduced monsoon precipitation in CMIP5 and CMIP6 projections (Wang et al., 2020; He et al., 2020; Hernandez and Chen, 2022; Ye and Wang, 2023).

Under SSP2-4.5, retreat is delayed in 5 of 6 monsoon regions in the multi-model mean (by 2.5–9 days; at least 3 of 4 models agree on the sign of this change in NAmerM, SAsiaM, EAsiaM and AusMCM), and onset advances by about 5 days in EAsiaM and 9 days in AusMCM (3 of 4 models; Fig. 3m and n), so that the season lengthens by about 8 days in EAsiaM (all 4 models) and 18 days in AusMCM (in 3 of 4 models). These timing changes are however rarely significant in individual models, so they indicate tendencies rather than robust shifts.

Relative to SSP2-4.5, G6-1.5K-SAI and G6-1.5K-HiLLA generally reduce active-season precipitation changes and, in some regions, reverse the sign of the response. This behavior is physically consistent with previous work showing that solar dimming and stratospheric aerosol forcing can weaken the hydrological cycle and reduce monsoon precipitation by suppressing surface warming, evaporation, and monsoon circulation (Bala et al., 2008; Tilmes et al., 2013; Bonou et al., 2023; Asutosh et al., 2025). G6-1.5K-MCB shows a different response from the two SAI strategies: in the multi-model mean, its active-season precipitation change is more positive than under both SAI strategies in all six regions (Fig. 3o). In the multi-model mean, G6-1.5K-MCB retains essentially all of the SSP2-4.5 increase in WAfriM (+8.4% versus +7.0%), most of it in SAsiaM (+4.1% versus +5.9%) and about 45% of it in EAsiaM (+4.4% versus +9.7%), whereas both SAI strategies produce decreases or near-zero changes in these regions (Table S1). The more positive active-season precipitation response under G6-1.5K-MCB is consistent with the distinct physical mechanism of MCB. Because MCB cools the climate by brightening marine low clouds rather than through stratospheric aerosol forcing, it cools the ocean more strongly than the land, which can shift the circulation and moisture transport toward land and increase land precipitation relative to SAI or greenhouse-gas forcing (Bala et al., 2011). A relatively wetter land monsoon response may therefore be a general feature of marine-cloud-based interventions rather than specific to this experiment, although its regional expression depends on where cloud brightening is applied (Hirasawa et al., 2026a) and differs among models (e.g., WAfriM decreases under G6-1.5K-MCB in CESM2 but increases in UKESM1 and E3SM).

https://doi.org/10.5194/egusphere-2026-6788
Preprint. Discussion started: 17 November 2026
© Author(s) 2026. CC BY 4.0 License.

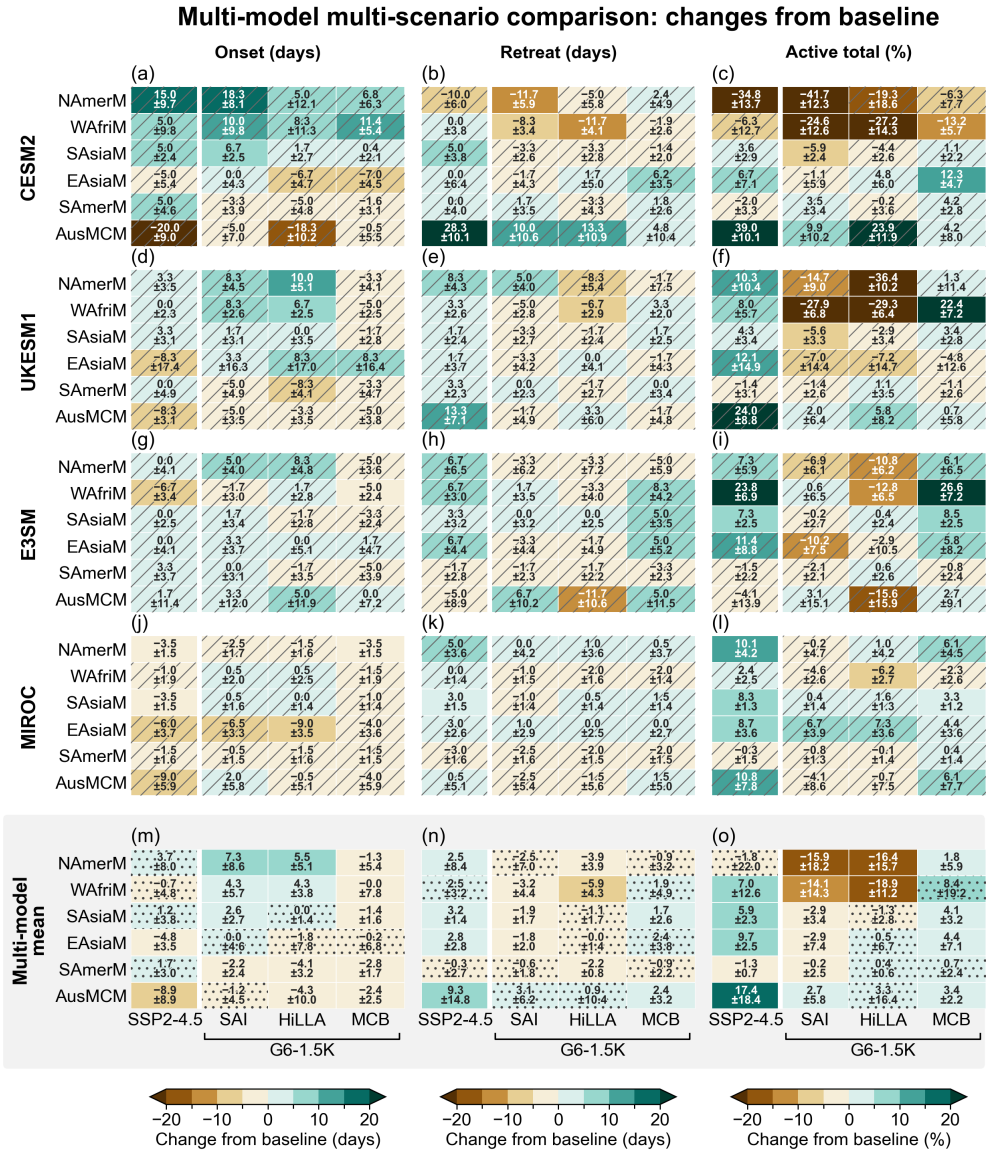


Figure 3. Multi-model, multi-scenario comparison of future monsoon changes across CESM2, UKESM1, E3SM, and MIROC. Panel rows correspond to models and columns correspond to monsoon metrics: onset change (days), retreat change (days), and active-season precipitation % change. Within each panel, rows show monsoon regions and columns show scenarios: SSP2-4.5, G6-1.5K-SAI, G6-1.5K-HiLLA, and G6-1.5K-MCB. Text annotations show the ensemble-mean change and one standard deviation derived from bootstrapping (intermodel standard deviation for the multi-model mean). Hatching indicates changes that are not statistically significant (95% hierarchical bootstrap interval includes zero). For the multi-model mean, dots indicate where fewer than 3 of 4 models share the sign of the multi-model mean.

https://doi.org/10.5194/egusphere-2026-6788
Preprint. Discussion started: 17 November 2026
© Author(s) 2026. CC BY 4.0 License.

The regional results also show that the monsoon response to SRM differs substantially across regions and models, and the regions can be grouped by how consistently the models respond. The most consistent response is found in WAfriM, where active-season precipitation decreases under SAI in 7 of the 8 model–SAI combinations (all except E3SM G6-1.5K-SAI, $+0.6\%$; Fig. 3c, f, i and l), in line with previous studies of SAI impacts on West African monsoon rainfall (Bonou et al., 2023; Da-Allada et al., 2020). Furthermore, the changes in 6 of these 8 model–SAI combinations are statistically significant. Under G6-1.5K-MCB, in contrast, the WAfriM response splits between models, with significant decreases in CESM2 (-13%) and significant increases in UKESM1 and E3SM ($+22$ and $+27\%$). NAmerM also shows a largely consistent SAI response: both SAI strategies reduce active-season precipitation in CESM2, UKESM1 and E3SM (-7 to -42%), whereas MIROC shows almost no change and G6-1.5K-MCB produces only small changes of either sign (-6 to $+6\%$; but all 4 models show no statistical significance).

In SAsiaM and EAsiaM, the sign of the active-season precipitation response under SAI depends on the model. For SAsiaM, Fig. 3c and f show reductions in active-season precipitation under both G6-1.5K-SAI and G6-1.5K-HiLLA in CESM2 and UKESM1. A possible explanation comes from previous work showing that SAI-induced lower-stratospheric warming can weaken the subtropical jet and alter upper-tropospheric wave activity, which in turn weakens the Asian Summer Monsoon Anticyclone and low-level monsoon circulation, enhances subsidence, and reduces moisture transport into South Asia, thereby suppressing mean and extreme summer monsoon precipitation (Asutosh et al., 2025). E3SM and MIROC, however, show near-zero changes or slight increases in active-season precipitation under the same SAI scenarios (-0.2 to $+1.6\%$; Fig. 3i and l), and all four models simulate increases under G6-1.5K-MCB ($+1$ to $+9\%$). In EAsiaM, all four models project increases under SSP2-4.5 ($+7$ to $+12\%$), but under the SAI strategies UKESM1 and E3SM simulate decreases (-3 to -10%), MIROC retains an increase ($+7\%$), and CESM2 changes little, so that the near-zero multi-model mean (Table S1) conceals responses of opposite sign. SAmerM, in contrast, shows a weak response under all scenarios, with changes within $\pm4\%$ and none statistically significant.

In AusMCM, the response to SRM depends on the strategy more than in any other region. G6-1.5K-SAI and G6-1.5K-MCB keep AusMCM close to its baseline climatology in all four models, with active-season precipitation changes of -4 to $+10\%$ and changes in season length of at most about two weeks, none of them statistically significant. G6-1.5K-HiLLA, in contrast, produces the widest intermodel spread: CESM2 simulates an onset 18 days earlier, a season 32 days longer and $+24\%$ active-season precipitation, whereas E3SM simulates a shorter season and a decrease (-17 days and -16%). These responses should be seen against the large SSP2-4.5 changes in this region, where onset advances by 8–20 days and the season lengthens by 10–48 days in 3 of 4 models, increasing active-season precipitation by 11–39% (significant only in CESM2). In the multi-model mean, all three strategies therefore offset most of the SSP2-4.5 increase to a similar degree ($+2.7$ to $+3.4\%$ versus $+17.4\%$; Table S1), but for G6-1.5K-HiLLA this near-zero mean reflects compensating responses of opposite sign in individual models rather than a consistent return to the baseline.

In the multi-model mean, all three SRM strategies bring monsoon metrics closer to the baseline climatology than SSP2-4.5. Averaged over the 36 region–metric combinations, the mean normalized departure from the baseline is 0.12 for G6-1.5K-SAI, 0.13 for G6-1.5K-HiLLA and 0.09 for G6-1.5K-MCB, compared with 0.16 for SSP2-4.5 (Table S2). G6-1.5K-MCB reduces

https://doi.org/10.5194/egusphere-2026-6788
Preprint. Discussion started: 17 November 2026
© Author(s) 2026. CC BY 4.0 License.

the magnitude of the SSP2-4.5 change in about three-quarters of the combinations (26 of 36), whereas G6-1.5K-SAI and G6-1.5K-HiLLA do so in just over half (19 and 20 of 36, respectively). The differences among strategies in the multi-model mean are therefore small, and they mask a clear split among models. In CESM2 and UKESM1, G6-1.5K-MCB is closest to the baseline most often (20 and 18 of 36; Table S2), whereas in E3SM G6-1.5K-SAI is closest most often (16 of 36 versus 6 for G6-1.5K-MCB). In MIROC, G6-1.5K-SAI and G6-1.5K-HiLLA perform similarly (12 and 16 of 36), and both outperform G6-1.5K-MCB (8 of 36). No single model reproduces the multi-model-mean ranking, and the strategy closest to the baseline in an individual model matches that of the multi-model mean in only 33–58% of combinations. Overall, these results indicate that SRM does not simply reverse or uniformly reduce SSP2-4.5 monsoon changes. Instead, the sign and magnitude of the responses depend strongly on region, metric, model and intervention strategy.

3.2 Historical model biases and intermodel spread

We show the multi-model range of historical biases relative to IMERG over 1998–2014 (1999–2014 for SAmerM and AusMCM; Fig. 4), providing a benchmark for historical model performance and for assessing whether projected changes are large relative to historical intermodel biases.

Historical model biases relative to IMERG are large compared with the projected monsoon responses (Fig. 4). In physical units (Sect. 2.2), the largest model bias exceeds the largest projected SRM change in 33 of the 36 region–metric combinations, by a median factor of 2.3 (Table S3). The exceptions are AusMCM onset and duration, where the largest SRM change exceeds the historical model bias, and SAsiaM peak timing, where both are 10 days (Fig. S5). Across models, the historical bias ranges span 12–47 days for the timing metrics (onset, retreat and peak timing), 20–63 days for duration, 28–105% of the observed value for active-season precipitation and 7–26% for wet-day intensity; they are widest in NAmerM and narrowest in SAsiaM and SAmerM. In several region–metric combinations all four models are biased in the same direction. All four models overestimate wet-day intensity in NAmerM, EAsiaM and SAmerM and simulate a later peak than IMERG in NAmerM and AusMCM. In SAmerM, every model also overestimates active-season precipitation and simulates an earlier peak and a later retreat (Fig. 4e), and in SAsiaM every model simulates a later onset and a shorter season than IMERG (Fig. 4c).

The bias ranges are largest in NAmerM, which has the widest range of the six regions for five of the six metrics, and in WAfriM, which has the second-widest range for duration (58 days) and active-season precipitation (77%) (Fig. 4a, b). In both regions, as in SAsiaM, the range of projected SRM responses is smaller than the historical bias range for every metric. Emergent-constraint studies show that historical model biases can propagate into future projection uncertainty; for example, Li et al. (2017) show that CMIP5 models with excessive historical precipitation biases over the tropical western Pacific also project systematically larger increases in Indian summer monsoon rainfall, such that correcting for this bias reduces the projected increase by nearly half. A large mean-state bias does not by itself imply an equally uncertain response, because a model can be biased and still simulate the forced change correctly. Across the four models, the size of a model's historical bias does not predict its projected response: the median rank correlation between bias and response across models is 0.00 for the mean SRM response and 0.20 for SSP2-4.5, and the most biased model is also the most responsive in only 8 of 36 combinations (9 would

https://doi.org/10.5194/egusphere-2026-6788
Preprint. Discussion started: 17 November 2026
© Author(s) 2026. CC BY 4.0 License.

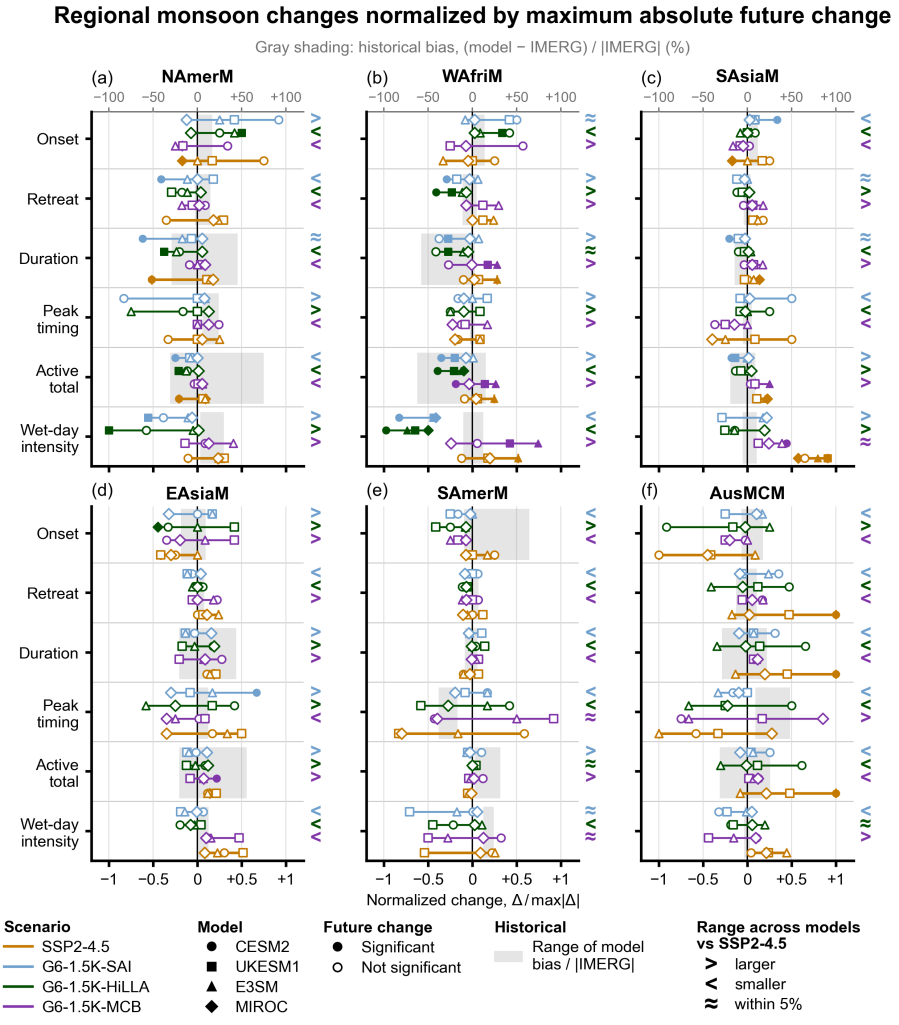


Figure 4. Regional monsoon response under future SSP2-4.5 and SRM scenarios across the six monsoon regions for onset, retreat, duration, peak timing, active-season precipitation, and wet-day intensity. For each metric, the change between each scenario and its baseline (Δ) is normalized by the maximum absolute change of that metric across models, scenarios, and regions ($\Delta/\max|\Delta|$), highlighting relative differences in response structure rather than absolute magnitude. Colors indicate scenarios: SSP2-4.5 (orange), G6-1.5K-SAI (light blue), G6-1.5K-HiLLA (dark green), and G6-1.5K-MCB (purple); marker shapes indicate models: CESM2 (circle), UKESM1 (square), E3SM (triangle), and MIROC (diamond). Filled markers denote statistically significant future changes, while open markers denote changes that are not statistically significant. Horizontal line segments show the intermodel spread for each scenario. Gray shading indicates the range of historical (1998–2014) model biases relative to IMERG, expressed as a percentage of the IMERG value (bias/|IMERG|); this differs from the normalization of the future changes, so the shading shows the sign and relative size of the historical biases. Text annotations indicate whether the future intermodel range is larger ($>$) or smaller ($<$) than the corresponding SSP2-4.5 range, with $\approx$ denoting ranges within 5% of each other.

https://doi.org/10.5194/egusphere-2026-6788
Preprint. Discussion started: 17 November 2026
© Author(s) 2026. CC BY 4.0 License.

be expected by chance). We find no comparable relationship between historical bias and projected response here, so whether these biases affect the projected SRM responses cannot be established from the present ensemble.

Across the two SAI experiments, intermodel spread is larger than under SSP2-4.5 for 27 (38%), smaller for 37 (51%), and comparable (within 5%) for the remaining 8 of the 72 region–metric combinations (Table S4). SAI appears to reduce the spread of model responses relative to SSP2-4.5, but its effect depends on the strategy and, above all, on the region. Increases are most pronounced in EAsiaM, where 8 of the 12 SAI and HiLLA cases show a larger intermodel range than SSP2-4.5 (Fig. 4d; Table S1). By contrast, AusMCM and SAmerM show the opposite behavior, with the majority of the cases (10 of 12 and 8 of 12, respectively) exhibiting a smaller intermodel range than SSP2-4.5 (Fig. 4f), while NAmerM, WAfriM and SAsiaM show no consistent tendency. Where SAI does increase the model spread, this is consistent with previous GeoMIP studies showing that SAI can introduce substantial regional precipitation uncertainty, particularly because precipitation and monsoon responses are sensitive to the spatial distribution of aerosol forcing and associated circulation shifts (Visioni et al., 2021). SAI also introduces sources of intermodel disagreement that are absent from the corresponding SSP2-4.5 simulations, including differences in how models transport and distribute the injected aerosols, the resulting latitudinal structure of aerosol optical depth, and the magnitude and pattern of aerosol-induced stratospheric heating, each of which feeds into the tropospheric circulation and precipitation response.

The intermodel spread under G6-1.5K-MCB shows a mixed pattern relative to SSP2-4.5: 17 of 36 region–metric combinations have a larger intermodel range, 16 have a smaller range, and 3 are comparable. Its regional pattern, however, differs from that of the SAI experiments. MCB reduces the intermodel spread in NAmerM (5 of 6 metrics), where SAI strategies show no consistent tendency, and in AusMCM (4 of 6), whereas it increases the spread in WAfriM (6 of 6) and, like the SAI strategies, in EAsiaM (4 of 6; Fig. 4 and Table S4).

Overall, our results show that the regional monsoon response to SRM depends strongly on both the intervention strategy and the climate model. The strategies also differ in how they affect intermodel spread: each increases the spread relative to SSP2-4.5 for 36–47% of region–metric combinations and reduces it for most of the remainder, with the sign depending mainly on the region. In 31 of 36 region–metric combinations, the largest historical model bias also exceeds the largest projected change under SSP2-4.5 or any SRM strategy. Four of the five exceptions are in AusMCM, where CESM2 projects particularly large changes under SSP2-4.5 (retreat, duration and active-season precipitation) and under G6-1.5K-HiLLA (onset and duration); in SAsiaM, the largest bias and the largest change in peak timing are equal (10 days). Historical model biases therefore generally exceed the projected responses. However, the size of a model's bias does not indicate the size of its response: across the 36 region–metric combinations, the model with the largest historical bias is also the model with the largest projected change in only 6 (SSP2-4.5) and 8 (averaged over the three SRM strategies) cases (Table S4).

3.3 Decomposing contributions to active-season precipitation changes

We next decompose changes in active-season precipitation to identify where changes in total active-season precipitation are primarily associated with shifts in the length of the monsoon season, the number of wet days, rainfall intensity on wet days, or effects captured by the residual term (Fig. 5). Because active-season precipitation is the rainfall accumulated between the

https://doi.org/10.5194/egusphere-2026-6788
Preprint. Discussion started: 17 November 2026
© Author(s) 2026. CC BY 4.0 License.

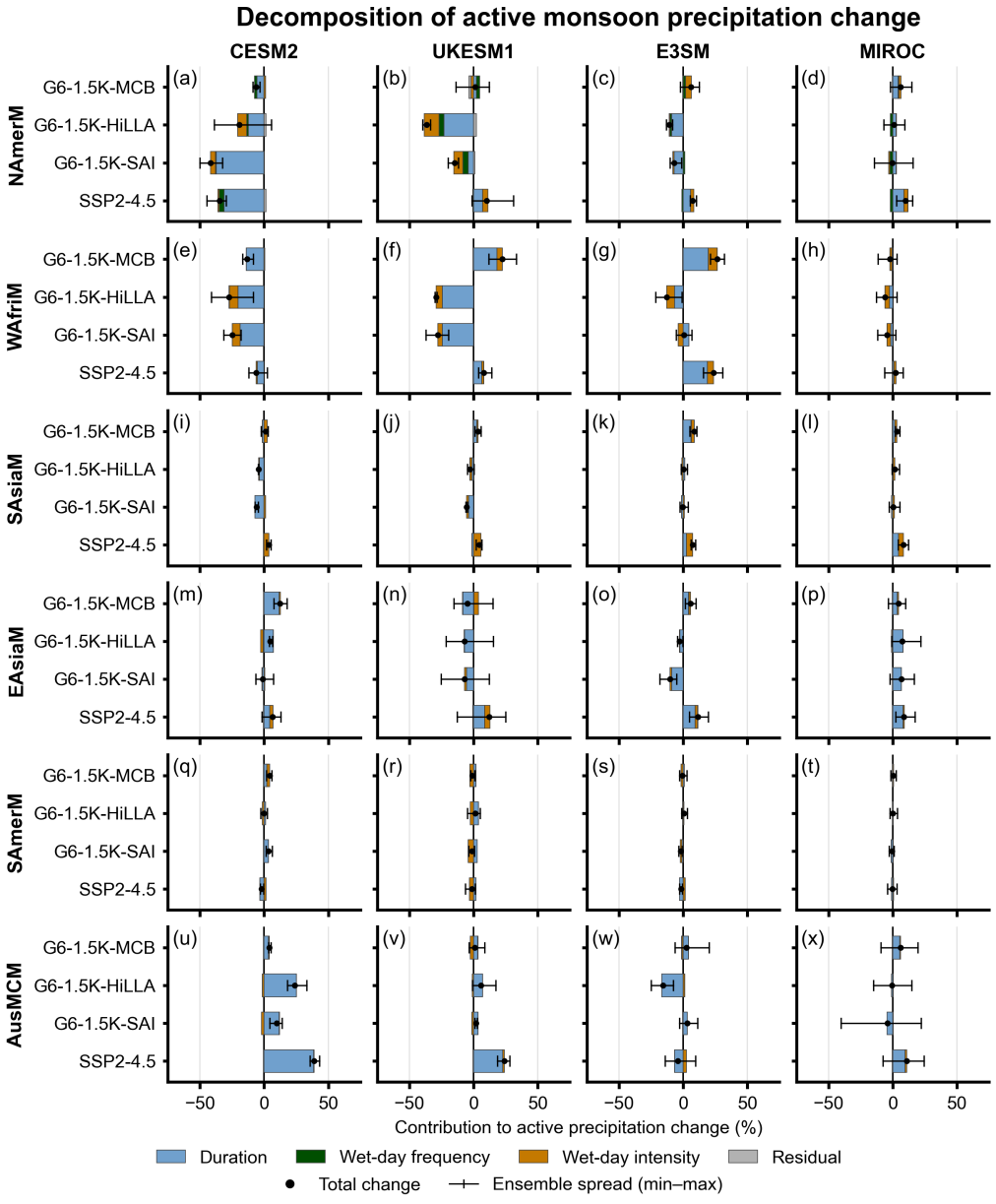


Figure 5. Decomposition of active-season precipitation changes into contributions from changes in active-season duration, wet-day frequency, wet-day intensity, and a residual term. Rows show monsoon regions, and columns show models. Within each panel, horizontally stacked bars show the percent contribution of each component to the total active-season precipitation change for each scenario relative to the 2020–2039 SSP2-4.5 reference period. Positive values indicate contributions that increase active-season precipitation, while negative values indicate contributions that decrease it. Black points denote the mean active-season precipitation change, and horizontal black lines show the ensemble min–max spread.

https://doi.org/10.5194/egusphere-2026-6788
Preprint. Discussion started: 17 November 2026
© Author(s) 2026. CC BY 4.0 License.

diagnosed onset and retreat, this decomposition is an accounting of the diagnosed metrics: a change in duration changes the integration window and therefore the total, even if the rainfall rate within the core season is unchanged.

Across most regions and models, duration is the largest of the three terms in 74 of the 96 model–region–scenario cases: 19 of 24 under SSP2-4.5 and 55 of 72 under the three SRM strategies. This behavior is particularly evident in NAmerM, WAfriM and AusMCM, and is clearest in CESM2, where the reduction in active-season precipitation under G6-1.5K-SAI and G6-1.5K-MCB in NAmerM and WAfriM coincides with a shorter monsoon season (Fig. 5a and e). Much of the change in active-season precipitation therefore reflects a shift in the diagnosed season boundaries rather than a change in rainfall rate. Seasonal totals over fixed calendar months would miss this shift in timing, which matters for growing seasons.

Despite this general tendency, the relative importance of the decomposition terms varies by region. In SAsiaM, active-season precipitation changes are small across most models and scenarios, consistent with the muted response identified in the normalized metric analysis (Fig. 4c). Where precipitation changes do occur, wet-day intensity contributes about as much as duration (it is the leading term in 7 of 16 cases, including the SSP2-4.5 response in CESM2, UKESM1, and E3SM; Fig. 5i–k). In contrast, NAmerM, WAfriM, and AusMCM show larger responses in which duration remains the primary contributor, while the secondary contributions from wet-day frequency and intensity differ among models (Fig. 5a–h, and u–x). This suggests broad agreement on the leading role of duration but less agreement on the mechanisms that modulate the response.

Overall, Fig. 5 shows that SRM-driven changes in active-season precipitation are, in most regions and models, led by changes in monsoon duration, with wet-day intensity and frequency as model-dependent secondary contributors: duration is the largest of the three terms in 74, wet-day intensity in 21, and wet-day frequency in 1 (in NAmerM) of 96 cases. Among all models, CESM2 represents the clearest example of duration-dominated behavior. The residual is small (up to about 2 percentage points; e.g., NAmerM in CESM2 and UKESM1; Fig. 5a and b). It is an accounting residual, arising from precipitation on days below the wet-day threshold and from averaging frequency and intensity separately, not an independently diagnosed process; its small size does not imply that the three terms capture all physical mechanisms of the precipitation change.

Moisture-budget analyses of monsoon precipitation change under warming consistently identify a thermodynamic contribution (e.g., the "wet-get-wetter" effect) that is partially offset by dynamic contributions from weakened monsoon circulation (Held and Soden, 2006; Chou et al., 2009; Endo and Kitoh, 2014). Under SRM, both terms are perturbed: stratospheric aerosol forcing cools the surface and reduces atmospheric moisture content, weakening the thermodynamic amplification, while aerosol-induced stratospheric heating and altered temperature gradients modify the circulation itself (Tilmes et al., 2013; Krishnamohan and Bala, 2022). Changes in these moisture-budget terms can alter rainfall within the active-season in ways that project onto duration, frequency, and intensity simultaneously or onto none of them cleanly and would therefore appear partly as residual in our framework. The presence of these residuals therefore serves as a caution: while this decomposition identifies the leading pathways of change in SRM-modified active-season precipitation, these components should be interpreted as first-order contributions rather than a complete additive budget, and model-region cases with large residuals warrant a more detailed examination of the sub-seasonal precipitation distribution and potentially a complementary moisture-budget decomposition into thermodynamic and dynamic terms before their responses are attributed to any single mechanism.

https://doi.org/10.5194/egusphere-2026-6788
Preprint. Discussion started: 17 November 2026
© Author(s) 2026. CC BY 4.0 License.

3.4 Model versus strategy dependence of monsoon changes

We next assess the relative contributions of model formulation and SRM strategy to the spread in projected monsoon changes using six standalone metrics: onset, retreat, duration, peak timing, active-season precipitation, and wet-day intensity. Wet-day frequency is evaluated separately as a component of the active-season precipitation in Fig. 5 and is therefore not included as a standalone metric in this comparison. Fig. 6 quantifies whether the uncertainty in regional monsoon changes is more strongly associated with differences among models or differences among SRM strategies. For each region and metric, Fig. 6a compares the magnitude of differences across models with the magnitude of differences across SRM scenarios. Specifically, for each SRM strategy we calculate the absolute difference in the projected change between every pair of models and average over the model pairs and then over the three strategies (model difference, M); likewise, for each model we average the absolute difference between every pair of SRM strategies and then average over the four models (strategy difference, S). Only the SRM experiments enter these differences; SSP2-4.5 is used only as the control from which each change is computed (see Text S1). The figure shows the ratio of these two mean pairwise differences. Fig. 6b provides a complementary sign-based metric, showing whether there is greater agreement in the sign of the projected change across models or across SRM scenarios.

Overall, model differences exceed scenario differences in the magnitude of the response for a majority of regions and metrics. In Fig. 6a, the model-difference/scenario-difference ratio exceeds one in 28 of the 36 region–metric combinations (78%). Model differences exceed SRM scenario differences for all six metrics in AusMCM and SAmerM, for 5 of 6 in NAmerM and WAfriM, and for 4 of 6 in EAsiaM (Fig. 6a). The prevalence of model-dominated responses is also consistent with the large spread in historical model biases shown in Fig. 4. NAmerM and WAfriM provide particularly clear examples: both exhibit large historical bias ranges and model differences exceeding scenario differences for 5 of 6 standalone metrics. More generally, the fact that historical intermodel biases are comparable to or larger than the projected responses for most region–metric combinations underscores that uncertainty in model formulation and mean-state monsoon representation remains an important component of uncertainty in regional SRM projections. This also aligns with conclusions from GeoMIP intercomparison studies that structural model uncertainty is a leading obstacle to confident regional assessment of SRM impacts (Visioni et al., 2021; Kravitz et al., 2013).

SAsiaM departs more clearly from this overall pattern, while EAsiaM shows a more mixed response (Fig. 6a). In SAsiaM, the differences between SRM scenarios exceed differences between models for 4 of 6 monsoon metrics (onset, duration, active-season precipitation and wet-day intensity) included in this comparison. This is consistent with the relatively muted and near-zero changes seen in the normalized metric analysis (Fig. 4): when the overall response is small, differences among SRM strategies can become more prominent relative to intermodel spread. However, because several model experiments include only three ensemble members, internal variability may contribute appreciably to both the apparent model and scenario differences, particularly for regions and metrics with weak responses.

This exception does not depend on the model versions used for MCB. When only UKESM1 and MIROC are compared, whose model versions are the same across the SAI and MCB experiments (for UKESM1, the MCB control differs only in omitting heterogeneous chemistry on stratospheric aerosols), strategy differences exceed model differences for 5 of the 6

https://doi.org/10.5194/egusphere-2026-6788
Preprint. Discussion started: 17 November 2026
© Author(s) 2026. CC BY 4.0 License.

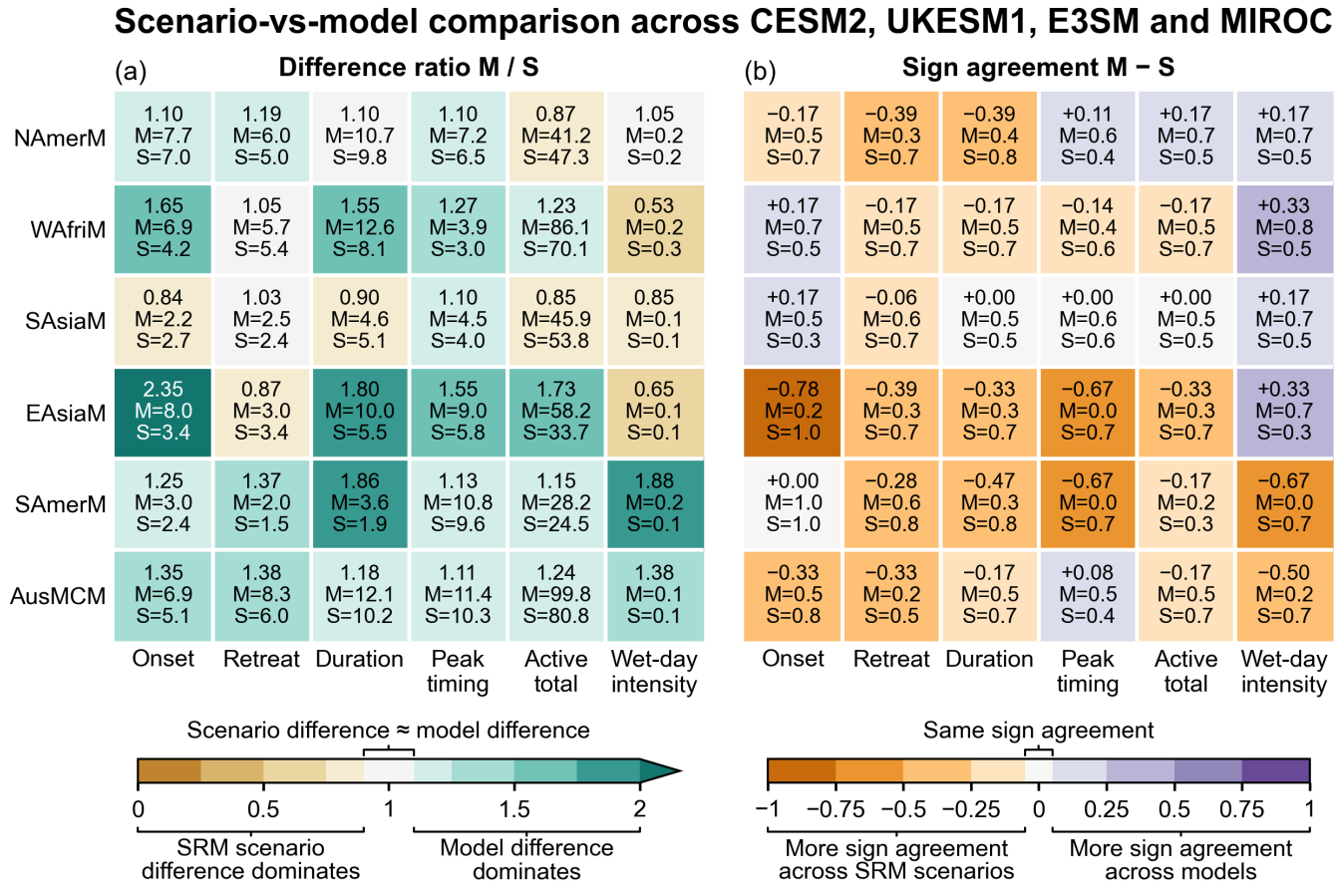


Figure 6. Comparison of model and SRM scenario dependence in projected monsoon changes across CESM2, UKESM1, E3SM, and MIROC for onset, retreat, duration, peak timing, active-season precipitation and wet-day intensity. Pairwise differences are calculated from the ensemble-mean change for each model–scenario combination; individual ensemble members are not treated as independent model or scenario realizations. (a) Left: Ratio of mean pairwise difference across models to the mean pairwise difference across scenarios for each monsoon region and metric. Values greater than 1 (teal) indicate that differences among models are larger than differences among SRM scenarios, while values less than 1 (brown) indicate that scenario differences dominate. (b) Right: the difference between sign robustness across models and sign robustness across scenarios, where sign agreement is defined as the fraction of pairwise comparisons with the same sign of change. Positive values (purple) indicate greater sign consistency across models, while negative values (orange) indicate greater sign consistency across scenarios. More details on the model-versus-scenario comparison in Text S1.

SAsiaM metrics, and in all four models MCB produces more active-season precipitation in SAsiaM than the mean of the two SAI strategies (by 2.3 to 8.4%; 7.6% in UKESM1 and 2.3% in MIROC). The SAsiaM results should therefore be interpreted

https://doi.org/10.5194/egusphere-2026-6788
Preprint. Discussion started: 17 November 2026
© Author(s) 2026. CC BY 4.0 License.

as indicating greater relative sensitivity to SRM strategy within the available simulations, rather than as a clean separation of strategy effects from internal variability.

The sign-agreement analysis in Fig. 6b adds an important nuance. Across the majority of the regions and metrics, the sign of the response is more consistent across SRM scenarios than across models. EAsiaM, SAmerM and AusMCM provide the clearest examples, with negative values for 5 of 6 metrics each. This indicates that the sign of the response is generally more consistent across SRM strategies within a model than across models. Thus, different SRM strategies often produce changes in the same direction within a given model, while models disagree more frequently on the direction of change.

The tendency toward greater sign agreement across SRM scenarios than across models is not uniform across regions. NAmerM, WAfriM and SAsiaM show weaker and more mixed sign-agreement behavior. In WAfriM, some metrics show greater sign agreement across models and others across SRM scenarios. In SAsiaM, only onset and wet-day intensity show greater sign agreement across models, retreat shows slightly greater agreement across scenarios, and the remaining three metrics show no difference. Together with the near-zero values for several metrics, this suggests that neither model choice nor SRM strategy consistently determines the sign of the response in these regions. Instead, the projected changes are relatively sensitive to both sources of uncertainty.

The scenario spread in Fig. 6 pools G6-1.5K-MCB with the two SAI strategies, although MCB differs from SAI in physical mechanism and forcing location and, for CESM2 and E3SM, in model version. Repeating the analysis with only the two SAI strategies, for which model configurations are identical, strengthens the dominance of model differences (ratio above one in 31 of 36 combinations; Fig. S6), so this result is not an artifact of pooling distinct interventions or model versions. In SAsiaM, however, scenario differences then dominate only onset (1 of 6 metrics, compared with 4 of 6 in Fig. 6a), indicating that its strong strategy dependence arises mainly from the inclusion of MCB. Nonetheless, the scenario spread would likely increase if more extreme or divergent SRM deployment strategies were included.

Internal variability is not formally separated from the model and scenario differences (Lehner et al., 2020), and several experiments include only three ensemble members. Using the spread among members as an estimate of sampling noise, model differences exceed the noise in 27 of 36 combinations and strategy differences in 23, but by median factors of only 1.4 and 1.2; a more conservative bootstrap estimate places both near the noise level. Across 2000 bootstrap replicates, the number of model-dominated combinations has a median of 24 (5–95% range 18–29) and exceeds half of the combinations in 92% of replicates, but only three individual cells are robust in at least 90% of replicates (model-dominated: SAmerM wet-day intensity and EAsiaM peak timing; strategy-dominated: WAfriM wet-day intensity). The count also depends on the models included (20–31 of 36 when one model is left out, with 20 without CESM2 and 21 without MIROC) and on the diagnostic choices (18–24 of 36 for alternative thresholds and numbers of Fourier harmonics; Table S5). The majority of model-dominated combinations is therefore robust as a summary, whereas most individual cells of Fig. 6a lie within sampling uncertainty. The most robust result is the dominance of model differences over differences between the two SAI strategies, which holds in 27–32 of 36 combinations in every test. Larger ensembles would be needed to separate internal variability from structural model uncertainty more rigorously (Tilmes et al., 2018; Milinski et al., 2020).

https://doi.org/10.5194/egusphere-2026-6788
Preprint. Discussion started: 17 November 2026
© Author(s) 2026. CC BY 4.0 License.

Overall, intermodel differences exceed inter-strategy differences for most region–metric combinations, particularly in AusMCM and SAmerM (all six metrics) and in NAmerM and WAfriM (5 of 6). Models differ mainly in the magnitude of the projected changes, whereas different SRM strategies often produce changes of the same sign within a given model, so robustness across strategies within one model does not imply robustness across models. Because the range of projected SRM responses across models is also smaller than the range of historical model biases in 33 of 36 combinations, projections from a single model should be interpreted with caution. Improving confidence in projected SRM monsoon impacts will therefore require reducing model mean-state biases and structural uncertainty, in addition to exploring a wider range of intervention strategies.

4 Conclusions

Understanding whether regional monsoon responses to SRM are robust across climate models and intervention strategies is critical because similar levels of global cooling can produce substantially different regional hydroclimate responses. Here, we provide a coordinated comparison of three GMSAT-targeted SRM strategies across multiple climate models and six major monsoon regions, evaluating both changes in monsoon seasonality and rainfall characteristics relative to a 2020–2039 SSP2-4.5 reference climate and the corresponding late-century SSP2-4.5 future. We assess monsoon onset, retreat, duration, peak timing, active-season precipitation, wet-day frequency, and wet-day intensity to determine how consistently these aspects of monsoon behavior respond across models and SRM strategies.

Overall, we find that SRM does not simply reverse or uniformly reduce the SSP2-4.5 monsoon response. The two SAI strategies generally dampen, and in WAfriM and SAsiaM reverse, the greenhouse-gas-driven increases in active-season precipitation, with similar overall magnitudes. G6-1.5K-MCB, however, retains more of the active-season precipitation increases in WAfriM, SAsiaM and EAsiaM, yet in the multi-model mean it departs least from the baseline across the six standalone metrics considered in the cross-model comparison.

Changes in monsoon rainfall under SRM are largely expressed through changes in seasonality. The decomposition of active-season precipitation shows that duration is most often the leading contributor (74 of 96 model–region–scenario cases), with wet-day intensity playing an important but more model-dependent secondary role and wet-day frequency contributing appreciably only in NAmerM. This implies that assessments based on seasonal-mean precipitation alone may conflate a shorter wet season with a weaker one, which has distinct consequences for agriculture, water storage, and flood risk. The residuals are small (at most about 2 percentage points), indicating that changes in active-season precipitation are well represented by changes in period-mean duration, wet-day frequency, and wet-day intensity; the remainder reflects precipitation on days below the wet-day threshold and covariance introduced by averaging the components separately.

Across the six standalone metrics, differences among models exceed differences among SRM strategies in 28 of 36 region–metric combinations, and in 31 of 36 for the two SAI strategies alone. The SAI-only result holds in every robustness test (27–32 of 36); with MCB included, it holds in most tests (18–31 of 36), but most individual combinations are not distinguishable from the sampling uncertainty of three-member ensembles. Model dependence is especially pronounced in SAmerM and AusMCM (for all six metrics); SAsiaM shows the opposite pattern when MCB is included, with strategy differences exceeding

https://doi.org/10.5194/egusphere-2026-6788
Preprint. Discussion started: 17 November 2026
© Author(s) 2026. CC BY 4.0 License.

model differences for 4 of 6 metrics considered. SRM also changes the intermodel spread relative to SSP2-4.5, increasing it in some regions (e.g., EAsiaM under SAI) and reducing it in others (e.g., AusMCM under SAI and NAmerM under MCB). Together, these results show that structural model differences are a major source of uncertainty in regional SRM projections.

The contrast in spread between MCB and SAI may partly reflect that G6-1.5K-MCB prescribed common geographic deployment regions across models, constraining one source of forcing-pattern uncertainty (Hirasawa et al., 2026b). In SAI, by contrast, aerosol transport, optical-depth distributions, and stratospheric heating can differ substantially among models (Niemeier and Tilmes, 2017; Visioni et al., 2021). MCB nevertheless retains model dependence through aerosol–cloud interactions, cloud susceptibility, and regional circulation feedbacks, despite model-specific calibration of sea salt emissions (Stjern et al., 2018; Rasch et al., 2024; Hirasawa et al., 2026b, c). Thus, MCB may remove one pathway for intermodel spread (i.e., the location of the forcing) while retaining uncertainty associated with the cloud response and regional circulation feedbacks, which may explain why it reduces the spread in some regions (e.g., NAmerM) but not in others. However, G6-1.5K-MCB does not reduce intermodel spread more systematically than the SAI strategies (larger in 17 and smaller in 16 of 36 combinations), suggesting that uncertainty in the cloud and circulation response outweighs the benefit of a common forcing location.

This dominance of model dependence occurs alongside large uncertainties in the simulated historical monsoon: the largest historical model bias relative to IMERG exceeds the largest projected SRM change in 33 of 36 region–metric combinations, typically by a factor of two, and the largest change under any scenario, including SSP2-4.5, in 31 of 36. Apparent differences among SRM strategies, or apparent robustness of a response within a single model, should therefore be interpreted cautiously when the underlying models disagree substantially in their historical monsoon climatology.

Several limitations should be considered when interpreting these results. First, most experiments include only three ensemble members, and many of the differences between models and strategies are comparable in magnitude to sampling uncertainty (Sect. 3.4). Second, the MCB and SAI experiments for CESM2 and E3SM use different model versions. Although the UKESM1–MIROC comparison suggests that this is unlikely to explain the main contrasts, its influence on individual regions cannot be ruled out. Third, the monsoon metrics are derived from regional-mean precipitation using fixed thresholds. While the dominance of model differences over differences between the two SAI strategies is robust to threshold changes of $\pm 20\%$ and to the use of 8 or 16 harmonics (27–32 of 36), the count including MCB varies between 18 and 24 of 36, and some changes in monsoon timing are comparable to the 5-day pentad resolution. Fourth, the three strategies represent only a subset of possible SRM designs, with two focused on SAI. The three strategies were deliberately designed to produce similar large-scale climate outcomes: all target the same GMSAT, their forcing is distributed with approximate hemispheric and zonal symmetry, and the midlatitude MCB emission regions were chosen specifically so that G6-1.5K-MCB reproduces the cooling pattern of G6-1.5K-SAI (Visioni et al., 2026; Hirasawa et al., 2026b). Therefore, including a broader range of strategies could reveal larger differences in scenario differences and their regional impacts. Finally, all experiments follow the same SSP2-4.5 trajectory for anthropogenic aerosols, land use, and other non-CO_2 forcings, which also influence monsoon behavior, particularly in Asia (Paul et al., 2016; Wilcox et al., 2020). Consequently, even SRM strategies that fully achieve their temperature targets would not necessarily restore all regional monsoon metrics to their 2020–2039 values.

https://doi.org/10.5194/egusphere-2026-6788
Preprint. Discussion started: 17 November 2026
© Author(s) 2026. CC BY 4.0 License.

Taken together, these results carry two implications for the assessment of SRM in the current generation of global climate models. First, improving and better constraining the historical simulations of regional monsoons, together with reducing structural model uncertainty, may be at least as important as expanding the range of intervention scenarios for improving confidence in projected SRM monsoon responses. Second, assessments of SRM hydroclimate impacts should extend beyond seasonal or annual precipitation totals and include evaluation of changes in monsoon seasonality, including onset, retreat, duration, and the distribution and intensity of rainfall within the active monsoon season. Future work should use larger ensembles to better characterize internal variability and extend this framework to multi-target deployment designs that explicitly constrain hemispheric temperature gradients. Subseasonal and moisture-budget decompositions would also help diagnose the residual precipitation responses.

Code and data availability. The monsoon metrics, changes, climatological pentad cycles, gridded monsoon-season precipitation totals and interhemispheric temperature gradients used in this study, for every model, experiment and ensemble member, are available at https://doi.org/10.5281/zenodo.23889423 (Wang, 2026). The G6-1.5K-SAI simulation data are available at https://doi.org/10.5281/zenodo.17613419 (Lee et al., 2025b). The CESM2(WACCM6) SSP2-4.5 simulation data are available at https://doi.org/10.5281/zenodo.6473954 (Richter and Visioni, 2022). G6-1.5K-HiLLA simulations in UKESM1, CESM2(WACCM6) and E3SMv3 are available at https://doi.org/10.5281/zenodo.17466720 (Duffey et al., 2025). The G6-1.5K-MCB simulation data can be found at https://doi.org/10.5281/zenodo.17525291 (Hirasawa et al., 2025). The UKESM1 SSP2-4.5 simulations are available from the JASMIN data server (https://gws-access.jasmin.ac.uk/public/macloud/). Historical simulations are available through the Earth System Grid Federation (https://esgf.llnl.gov). GPM IMERG V07 daily precipitation is available from the NASA Goddard Earth Sciences Data and Information Services Center (https://doi.org/10.5067/GPM/IMERGDF/DAY/07; Huffman et al., 2023b).

Author contributions. CW conducted the analysis. DV provided guidance on the structure and analysis. BC, ZML and BTJ provided feedback on the analysis. MH, WL and HH provided the simulations and feedback on the analysis. CW prepared the manuscript with assistance from all co-authors.

Competing interests. The authors declare there are no conflicts of interest for this manuscript.

Financial support. CW, DV, and WL acknowledge financial support by the Quadrature Charitable Foundation. Support for MH was provided by SilverLining's Safe Climate Research Initiative (SCRI).

Acknowledgements. We would like to thank the internal reviewer at Climate Central. We would like to acknowledge the high-performance computing support from the Derecho system (doi:10.5065/qx9a-pg09) provided by the NSF National Center for Atmospheric Research (NCAR), sponsored by the National Science Foundation.

https://doi.org/10.5194/egusphere-2026-6788
Preprint. Discussion started: 17 November 2026
© Author(s) 2026. CC BY 4.0 License.

References

Alterskjær, K. and Kristjánsson, J.: The sign of the radiative forcing from marine cloud brightening depends on both particle size and injection amount, Geophysical Research Letters, 40, 210–215, https://doi.org/10.1029/2012GL054286, 2013.

Asutosh, A., Tilmes, S., Bednarz, E. M., and Fadnavis, S.: South Asian Summer Monsoon under stratospheric aerosol intervention, npj Climate and Atmospheric Science, 8, 3, https://doi.org/10.1038/s41612-024-00875-z, 2025.

Bala, G., Duffy, P., and Taylor, K.: Impact of geoengineering schemes on the global hydrological cycle, Proceedings of the National Academy of Sciences, 105, 7664–7669, https://doi.org/10.1073/pnas.0711648105, 2008.

Bala, G., Caldeira, K., Nemani, R., Cao, L., Ban-Weiss, G., and Shin, H.-J.: Albedo enhancement of marine clouds to counteract global warming: impacts on the hydrological cycle, Climate dynamics, 37, 915–931, https://doi.org/10.1007/s00382-010-0868-1, 2011.

Baughman, E., Gnanadesikan, A., DeGaetano, A., and Adcroft, A.: Investigation of the surface and circulation impacts of cloud-brightening geoengineering, Journal of Climate, 25, 7527–7543, https://doi.org/10.1175/JCLI-D-11-00282.1, 2012.

Bonou, F., Da-Allada, C. Y., Baloitcha, E., Alamou, E., Biao, E. I., Zandagba, J., Obada, E., Pomalegni, Y., Irvine, P. J., and Tilmes, S.: Stratospheric sulfate aerosols impacts on West African monsoon precipitation using GeoMIP models, Earth's Future, 11, https://doi.org/10.1029/2023EF003779, 2023.

Bronstert, A., Niehoff, D., and Schiffler, G. R.: Modelling infiltration and infiltration excess: The importance of fast and local processes, Hydrological Processes, 37, e14 875, https://doi.org/10.1002/hyp.14875, 2023.

Chen, C.-C., Richter, J. H., Lee, W. R., MacMartin, D. G., and Kravitz, B.: Rethinking the susceptibility-based strategy for marine cloud brightening climate intervention: Experiment with CESM2 and its implications, Geophysical Research Letters, 51, e2024GL108 860, https://doi.org/10.1029/2024GL108860, 2024.

Chou, C., Neelin, J. D., Chen, C.-A., and Tu, J.-Y.: Evaluating the "rich-get-richer" mechanism in tropical precipitation change under global warming, Journal of climate, 22, 1982–2005, https://doi.org/10.1175/2008JCLI2471.1, 2009.

Da-Allada, C. Y., Baloïtcha, E., Alamou, E., Awo, F., Bonou, F., Pomalegni, Y., Biao, E., Obada, E., Zandagba, J., Tilmes, S., et al.: Changes in West African summer monsoon precipitation under stratospheric aerosol geoengineering, Earth's Future, 8, e2020EF001 595, https://doi.org/10.1029/2020EF001595, 2020.

Danabasoglu, G., Lamarque, J.-F., Bacmeister, J., Bailey, D., DuVivier, A., Edwards, J., Emmons, L., Fasullo, J., Garcia, R., Gettelman, A., et al.: The community earth system model version 2 (CESM2), Journal of Advances in Modeling Earth Systems, 12, e2019MS001 916, https://doi.org/10.1029/2019MS001916, 2020.

Douville, H., Raghavan, K., Renwick, J., Allan, R. P., Arias, P. A., Barlow, M., Cerezo-Mota, R., Cherchi, A., Gan, T. Y., Gergis, J., Jiang, D., Khan, A., Pokam Mba, W., Rosenfeld, D., Tierney, J., and Zolina, O.: Water Cycle Changes, in: Climate Change 2021: The Physical Science Basis. Contribution of Working Group I to the Sixth Assessment Report of the Intergovernmental Panel on Climate Change, edited by Masson-Delmotte, V., Zhai, P., Pirani, A., Connors, S. L., Péan, C., Berger, S., Caud, N., Chen, Y., Goldfarb, L., Gomis, M. I., Huang, M., Leitzell, K., Lonnoy, E., Matthews, J. B. R., Maycock, T. K., Waterfield, T., Yelekçi, O., Yu, R., and Zhou, B., pp. 1055–1210, Cambridge University Press, Cambridge, United Kingdom and New York, NY, USA, https://doi.org/10.1017/9781009157896.010, 2021.

Duffey, A., Wheeler, L., and Lee, W.: HiLLA-SAI simulations in UKESM1, CESM2-WACCM and E3SMv3, Zenodo [Dataset], https://doi.org/10.5281/zenodo.17466720, 2025.

https://doi.org/10.5194/egusphere-2026-6788
Preprint. Discussion started: 17 November 2026
© Author(s) 2026. CC BY 4.0 License.

Duffey, A., Lee, W., Wheeler, L., Irvine, P., Wagman, B., Henry, M., Visioni, D., Tsamados, M., and MacMartin, D.: The global climate response to High-Latitude Low-Altitude Stratospheric Aerosol Injection (HiLLA-SAI), Earth System Dynamics, 17, 353–385, https://doi.org/10.5194/esd-17-353-2026, 2026.

Endo, H. and Kitoh, A.: Thermodynamic and dynamic effects on regional monsoon rainfall changes in a warmer climate, Geophysical Research Letters, 41, 1704–1711, https://doi.org/10.1002/2013GL059158, 2014.

Evans, S., Marchand, R., and Ackerman, T.: Variability of the Australian monsoon and precipitation trends at Darwin, Journal of Climate, 27, 8487–8500, https://doi.org/10.1175/JCLI-D-13-00422.1, 2014.

Gabriel, Martins Ribeiro, J., Reboita, M. S., and Visioni, D.: South America monsoon lifecycle under SAI and no-SAI scenarios in a warming world, Environmental Research: Climate, https://doi.org/10.1088/2752-5295/ae42df, 2026.

Gadgil, S. and Gadgil, S.: The Indian monsoon, GDP and agriculture, Economic and political weekly, pp. 4887–4895, https://doi.org/10.2307/4418949, 2006.

Gettelman, A., Mills, M., Kinnison, D., Garcia, R., Smith, A., Marsh, D., Tilmes, S., Vitt, F., Bardeen, C., McInerny, J., et al.: The whole atmosphere community climate model version 6 (WACCM6), Journal of Geophysical Research: Atmospheres, 124, 12 380–12 403, https://doi.org/10.1029/2019JD030943, 2019.

Golaz, J.-C., Van Roekel, L. P., Zheng, X., Roberts, A. F., Wolfe, J. D., Lin, W., Bradley, A. M., Tang, Q., Maltrud, M. E., Forsyth, R. M., et al.: The DOE E3SM model version 2: Overview of the physical model and initial model evaluation, Journal of Advances in Modeling Earth Systems, 14, e2022MS003 156, https://doi.org/10.1029/2022MS003156, 2022.

Golaz, J.-C., Lin, W., Zheng, X., Xie, S., Roberts, A. F., Van Roekel, L. P., Thornton, P. E., Barthel, A. M., Bradley, A. M., Wolfe, J. D., et al.: The Energy Exascale Earth System Model Version 3: 2. Overview of the Coupled System, Journal of Advances in Modeling Earth Systems, 18, e2025MS005 302, https://doi.org/10.1029/2025MS005302, 2026.

Haywood, J. M., Jones, A., Jones, A. C., Halloran, P., and Rasch, P. J.: Climate intervention using marine cloud brightening (MCB) compared with stratospheric aerosol injection (SAI) in the UKESM1 climate model, Atmospheric Chemistry and Physics, 23, 15 305–15 324, https://doi.org/10.5194/acp-23-15305-2023, 2023.

He, C., Li, T., and Zhou, W.: Drier North American monsoon in contrast to Asian–African monsoon under global warming, Journal of Climate, 33, 9801–9816, https://doi.org/10.1175/JCLI-D-20-0189.1, 2020.

Held, I. M. and Soden, B. J.: Robust responses of the hydrological cycle to global warming, Journal of climate, 19, 5686–5699, https://doi.org/10.1175/JCLI3990.1, 2006.

Hernandez, M. and Chen, L.: Future land precipitation changes over the North American monsoon region using CMIP5 and CMIP6 simulations, Journal of Geophysical Research: Atmospheres, 127, e2021JD035 911, https://doi.org/10.1029/2021JD035911, 2022.

Hill, S. and Ming, Y.: Nonlinear climate response to regional brightening of tropical marine stratocumulus, Geophysical Research Letters, 39, https://doi.org/10.1029/2012GL052064, 2012.

Hirasawa, H., Matthew, H., Wood, R., Doherty, S., and Rasch, P.: Data for "G6-1.5K-MCB: Marine Cloud Brightening Scenario design for the Geoengineering Model Intercomparison Project (GeoMIP), Zenodo [Dataset]", https://doi.org/10.5281/zenodo.17525291, 2025.

Hirasawa, H., Henry, M., Mason, A. M., Rasch, P. J., Doherty, S. J., Wood, R., Haywood, J., and Von Salzen, K.: Forcing susceptibility and climate sensitivity to midlatitude marine cloud brightening, Journal of Climate, 39, 769–784, https://doi.org/10.1175/JCLI-D-25-0337.1, 2026a.

https://doi.org/10.5194/egusphere-2026-6788
Preprint. Discussion started: 17 November 2026
© Author(s) 2026. CC BY 4.0 License.

Hirasawa, H., Henry, M., Rasch, P. J., Wood, R., Doherty, S. J., Haywood, J., Wong, A., Lamarque, J.-F., Brody, E., and Wang, H.: G6-1.5 K-MCB: Marine Cloud Brightening scenario design for the Geoengineering Model Intercomparison Project (GeoMIP) in CESM2. 1, E3SMv2. 0, and UKESM1. 1, Geoscientific Model Development, 19, 3257–3283, https://doi.org/10.5194/gmd-19-3257-2026, 2026b.

Hirasawa, H., von Salzen, K., Henry, M., Smith, J., Bender, F. A.-M., Wang, C., Doherty, S., Wood, R., Rasch, P. J., and Haywood, J.: On the Range of Marine Cloud Brightening Radiative Forcing across Earth System Models, EGUsphere, 2026, 1–31, https://doi.org/10.5194/egusphere-2026-5460, 2026c.

Huang, W.-R., Chang, Y.-H., Deng, L., and Liu, P.-Y.: Simulation and projection of summer convective afternoon rainfall activities over Southeast Asia in CMIP6 models, Journal of Climate, 34, 5001–5016, https://doi.org/10.1175/JCLI-D-20-0788.1, 2021.

Huffman, G. J., Bolvin, D. T., Joyce, R., Nelkin, E. J., Tan, J., Braithwaite, D., Hsu, K., Kelley, O. A., Nguyen, P., Sorooshian, S., Watters, D. C., West, B. J., and Xie, P.: NASA Global Precipitation Measurement (GPM) Integrated Multi-satellitE Retrievals for GPM (IMERG) Version 07, Algorithm theoretical basis document, NASA Goddard Space Flight Center, Greenbelt, MD, USA, https://gpm.nasa.gov/resources/documents/imerg-v07-atbd, 2023a.

Huffman, G. J., Stocker, E. F., Bolvin, D. T., Nelkin, E. J., and Tan, J.: GPM IMERG Final Precipitation L3 1 day 0.1 degree x 0.1 degree V07, https://doi.org/10.5067/GPM/IMERGDF/DAY/07, dataset, accessed 4 November 2026, 2023b.

IPCC: Summary for Policymakers, in: Climate Change 2021: The Physical Science Basis. Contribution of Working Group I to the Sixth Assessment Report of the Intergovernmental Panel on Climate Change, edited by Masson-Delmotte, V., Zhai, P., Pirani, A., Connors, S. L., Péan, C., Berger, S., Caud, N., Chen, Y., Goldfarb, L., Gomis, M. I., Huang, M., Leitzell, K., Lonnoy, E., Matthews, J. B. R., Maycock, T. K., Waterfield, T., Yelekçi, O., Yu, R., and Zhou, B., pp. 3–32, Cambridge University Press, Cambridge, United Kingdom and New York, NY, USA, https://doi.org/10.1017/9781009157896.001, 2021.

Iturbide, M., Gutiérrez, J. M., Alves, L. M., Bedia, J., Cimadevilla, E., Cofiño, A. S., Cerezo-Mota, R., Di Luca, A., Faria, S. H., Gorodetskaya, I., et al.: An update of IPCC climate reference regions for subcontinental analysis of climate model data: definition and aggregated datasets, Earth System Science Data Discussions, 2020, 1–16, https://doi.org/10.5194/essd-12-2959-2020, 2020.

Janowiak, J. E. and Xie, P.: A global-scale examination of monsoon-related precipitation, Journal of climate, 16, 4121–4133, https://doi.org/10.1175/1520-0442(2003)016<4121:AGEOMP>2.0.CO;2, 2003.

Jin, C., Wang, B., and Liu, J.: Future changes and controlling factors of the eight regional monsoons projected by CMIP6 models, Journal of Climate, 33, 9307–9326, https://doi.org/10.1175/JCLI-D-20-0236.1, 2020.

Jones, A., Haywood, J., and Boucher, O.: Climate impacts of geoengineering marine stratocumulus clouds, Journal of Geophysical Research: Atmospheres, 114, https://doi.org/10.1029/2008JD011450, 2009.

Kawamiya, M., Hajima, T., Tachiiri, K., Watanabe, S., and Yokohata, T.: Two decades of Earth system modeling with an emphasis on Model for Interdisciplinary Research on Climate (MIROC), Progress in Earth and Planetary Science, 7, 1–13, https://doi.org/10.1186/s40645-020-00369-5, 2020.

Knapp, A. K., Beier, C., Briske, D. D., Classen, A. T., Luo, Y., Reichstein, M., Smith, M. D., Smith, S. D., Bell, J. E., Fay, P. A., et al.: Consequences of more extreme precipitation regimes for terrestrial ecosystems, Bioscience, 58, 811–821, https://doi.org/10.1641/B580908, 2008.

Kravitz, B., Caldeira, K., Boucher, O., Robock, A., Rasch, P. J., Alterskjaer, K., Karam, D. B., Cole, J. N., Curry, C. L., Haywood, J. M., et al.: Climate model response from the geoengineering model intercomparison project (GeoMIP), Journal of Geophysical Research: Atmospheres, 118, 8320–8332, https://doi.org/10.1002/jgrd.50646, 2013.

https://doi.org/10.5194/egusphere-2026-6788
Preprint. Discussion started: 17 November 2026
© Author(s) 2026. CC BY 4.0 License.



Krishnamohan, K. and Bala, G.: Sensitivity of tropical monsoon precipitation to the latitude of stratospheric aerosol injections, Climate Dynamics, 59, 151–168, https://doi.org/10.1007/s00382-021-06121-z, 2022.

Latham, J., Rasch, P., Chen, C.-C., Kettles, L., Gadian, A., Gettelman, A., Morrison, H., Bower, K., and Choularton, T.: Global temperature stabilization via controlled albedo enhancement of low-level maritime clouds, Philosophical Transactions of the Royal Society A: Mathematical, Physical and Engineering Sciences, 366, 3969–3987, https://doi.org/10.1098/rsta.2008.0137, 2008.

Lee, W. R., Chen, C.-C., Richter, J., MacMartin, D. G., and Kravitz, B.: First simulations of feedback algorithm-regulated marine cloud brightening, Geophysical Research Letters, 52, e2024GL113 728, https://doi.org/10.1029/2024GL113728, 2025a.

Lee, W. R., Visioni, D., Wagman, B. M., Wentland, C. R., Kravitz, B., Watanabe, S., Sekiya, T., Jones, A., Haywood, J., Henry, M., and Bednarz, E. M.: Data for "G6-1.5K-SAI and G6sulfur: changes in impacts and uncertainty depending on stratospheric aerosol injection strategy in the Geoengineering Model Intercomparison Project, Zenodo [Dataset]", https://doi.org/10.5281/zenodo.17613419, 2025b.

Lee, W. R., Visioni, D., Wagman, B. M., Wentland, C. R., Kravitz, B., Watanabe, S., Sekiya, T., Jones, A., Haywood, J., Henry, M., et al.: G6-1.5 K-SAI and G6sulfur: changes in impacts and uncertainty depending on stratospheric aerosol injection strategy in the Geoengineering Model Intercomparison Project, Atmospheric Chemistry and Physics, 26, 7463–7483, https://doi.org/10.5194/acp-26-7463-2026, 2026.

Lehner, F., Deser, C., Maher, N., Marotzke, J., Fischer, E. M., Brunner, L., Knutti, R., and Hawkins, E.: Partitioning climate projection uncertainty with multiple large ensembles and CMIP5/6, Earth System Dynamics, 11, 491–508, https://doi.org/10.5194/esd-11-491-2020, 2020.

Li, G., Xie, S.-P., He, C., and Chen, Z.: Western Pacific emergent constraint lowers projected increase in Indian summer monsoon rainfall, Nature Climate Change, 7, 708–712, https://doi.org/10.1038/nclimate3387, 2017.

LinHo, L., Huang, X., and Lau, N.-C.: Winter-to-spring transition in East Asia: A planetary-scale perspective of the South China spring rain onset, Journal of Climate, 21, 3081–3096, https://doi.org/10.1175/2007JCLI1611.1, 2008.

Milinski, S., Maher, N., and Olonscheck, D.: How large does a large ensemble need to be?, Earth System Dynamics, 11, 885–901, https://doi.org/10.5194/esd-11-885-2020, 2020.

Mulcahy, J. P., Jones, C. G., Rumbold, S. T., Kuhlbrodt, T., Dittus, A. J., Blockley, E. W., Yool, A., Walton, J., Hardacre, C., Andrews, T., et al.: UKESM1. 1: development and evaluation of an updated configuration of the UK Earth System Model, Geoscientific Model Development, 16, 1569–1600, https://doi.org/10.5194/gmd-16-1569-2023, 2023.

Muñoz-Sanchez, R., Ordoñez, P., Gallego, D., and Ochoa-Moya, C. A.: An objective procedure for rainy season onset and withdrawal dates over the Mexico Valley Basin: R. Muñoz-Sanchez et al., Theoretical and Applied Climatology, 155, 1667–1678, https://doi.org/10.1007/s00704-023-04714-8, 2024.

Nakaegawa, T., Arakawa, O., and Kamiguchi, K.: Investigation of climatological onset and withdrawal of the rainy season in Panama based on a daily gridded precipitation dataset with a high horizontal resolution, Journal of Climate, 28, 2745–2763, https://doi.org/10.1175/JCLI-D-14-00243.1, 2015.

Niemeier, U. and Tilmes, S.: Sulfur injections for a cooler planet, Science, 357, 246–248, https://doi.org/10.1126/science.aan3317, 2017.

Odoulami, R. C., Hirasawa, H., Kouadio, K., Patel, T. D., Quagraine, K. A., Pinto, I., Egbebiyi, T. S., Abiodun, B. J., Lennard, C., and New, M. G.: Africa's climate response to Marine Cloud Brightening strategies is highly sensitive to deployment region, Journal of Geophysical Research: Atmospheres, 129, e2024JD041 070, https://doi.org/10.1029/2024JD041070, 2024.

O'Neill, B. C., Tebaldi, C., van Vuuren, D. P., Eyring, V., Friedlingstein, P., Hurtt, G., Knutti, R., Kriegler, E., Lamarque, J.-F., Lowe, J., et al.: The Scenario Model Intercomparison Project (ScenarioMIP) for CMIP6, Geoscientific Model Development, https://doi.org/10.5194/gmd-9-3461-2016, 2016.

https://doi.org/10.5194/egusphere-2026-6788
Preprint. Discussion started: 17 November 2026
© Author(s) 2026. CC BY 4.0 License.

Paul, S., Ghosh, S., Oglesby, R., Pathak, A., Chandrasekharan, A., and Ramsankaran, R.: Weakening of Indian summer monsoon rainfall due to changes in land use land cover, Scientific reports, 6, 32 177, https://doi.org/10.1038/srep32177, 2016.

Prakash, S., Mitra, A. K., AghaKouchak, A., Liu, Z., Norouzi, H., and Pai, D.: A preliminary assessment of GPM-based multi-satellite precipitation estimates over a monsoon dominated region, Journal of Hydrology, 556, 865–876, https://doi.org/10.1016/j.jhydrol.2016.01.029, 2018.

Rasch, P. J., Tilmes, S., Turco, R. P., Robock, A., Oman, L., Chen, C.-C., Stenchikov, G. L., and Garcia, R. R.: An overview of geoengineering of climate using stratospheric sulphate aerosols, Philosophical Transactions of the Royal Society A: Mathematical, Physical and Engineering Sciences, 366, 4007–4037, https://doi.org/10.1098/rsta.2008.0131, 2008.

Rasch, P. J., Hirasawa, H., Wu, M., Doherty, S. J., Wood, R., Wang, H., Jones, A., Haywood, J., and Singh, H.: A protocol for model intercomparison of impacts of marine cloud brightening climate intervention, Geoscientific Model Development, 17, 7963–7994, https://doi.org/10.5194/gmd-17-7963-2024, 2024.

Richter, J. H. and Visioni, D.: SSP2-4.5 Simulations with CESM2 (WACCM6), Zenodo [Dataset], https://doi.org/10.5281/zenodo.6473954, 2022.

Robock, A., Oman, L., and Stenchikov, G. L.: Regional climate responses to geoengineering with tropical and Arctic SO2 injections, Journal of Geophysical Research: Atmospheres, 113, https://doi.org/10.1029/2008JD010050, 2008.

Robock, A., Marquardt, A., Kravitz, B., and Stenchikov, G.: Benefits, risks, and costs of stratospheric geoengineering, Geophysical research letters, 36, https://doi.org/10.1029/2009GL039209, 2009.

Roose, S., Bala, G., Krishnamohan, K., Cao, L., and Caldeira, K.: Quantification of tropical monsoon precipitation changes in terms of interhemispheric differences in stratospheric sulfate aerosol optical depth, Climate Dynamics, 61, 4243–4258, https://doi.org/10.1007/s00382-023-06799-3, 2023.

Sellar, A. A., Jones, C. G., Mulcahy, J. P., Tang, Y., Yool, A., Wiltshire, A., O'connor, F. M., Stringer, M., Hill, R., Palmieri, J., et al.: UKESM1: Description and evaluation of the UK Earth System Model, Journal of Advances in Modeling Earth Systems, 11, 4513–4558, https://doi.org/10.1029/2019MS001739, 2019.

Seregina, L. S., Fink, A. H., van der Linden, R., Elagib, N. A., and Pinto, J. G.: A new and flexible rainy season definition: Validation for the Greater Horn of Africa and application to rainfall trends, International Journal of Climatology, 39, 989–1012, https://doi.org/10.1002/joc.5856, 2019.

Singh, M., Bala, G., and Seshadri, A. K.: An investigation of the characteristics of Indian Summer monsoon low-pressure systems under stratospheric aerosol geoengineering, Earth's Future, 14, e2026EF009 141, https://doi.org/10.1029/2026EF009141, 2026.

Stjern, C. W., Muri, H., Ahlm, L., Boucher, O., Cole, J. N., Ji, D., Jones, A., Haywood, J., Kravitz, B., Lenton, A., et al.: Response to marine cloud brightening in a multi-model ensemble, Atmospheric Chemistry and Physics, 18, 621–634, https://doi.org/10.5194/acp-18-621-2018, 2018.

Sun, W., Wang, B., Chen, D., Gao, C., Lu, G., and Liu, J.: Global monsoon response to tropical and Arctic stratospheric aerosol injection, Climate Dynamics, 55, 2107–2121, https://doi.org/10.1007/s00382-020-05371-7, 2020.

Tilmes, S., Fasullo, J., Lamarque, J.-F., Marsh, D. R., Mills, M., Alterskjaer, K., Muri, H., Kristjánsson, J. E., Boucher, O., Schulz, M., et al.: The hydrological impact of geoengineering in the Geoengineering Model Intercomparison Project (GeoMIP), Journal of Geophysical Research: Atmospheres, 118, 11–036, https://doi.org/10.1002/jgrd.50868, 2013.

https://doi.org/10.5194/egusphere-2026-6788
Preprint. Discussion started: 17 November 2026
© Author(s) 2026. CC BY 4.0 License.

Tilmes, S., Richter, J. H., Kravitz, B., MacMartin, D. G., Mills, M. J., Simpson, I. R., Glanville, A. S., Fasullo, J. T., Phillips, A. S., Lamarque, J.-F., et al.: CESM1(WACCM) stratospheric aerosol geoengineering large ensemble project, Bulletin of the American Meteorological Society, 99, 2361–2371, https://doi.org/10.1175/BAMS-D-17-0267.1, 2018.

Turner, A. G. and Annamalai, H.: Climate change and the South Asian summer monsoon, Nature Climate Change, 2, 587–595, https://doi.org/10.1038/nclimate1495, 2012.

Visioni, D., MacMartin, D. G., Kravitz, B., Boucher, O., Jones, A., Lurton, T., Martine, M., Mills, M. J., Nabat, P., Niemeier, U., et al.: Identifying the sources of uncertainty in climate model simulations of solar radiation modification with the G6sulfur and G6solar Geoengineering Model Intercomparison Project (GeoMIP) simulations, Atmospheric Chemistry and Physics, 21, 10 039–10 063, https://doi.org/10.5194/acp-21-10039-2021, 2021.

Visioni, D., Robock, A., Haywood, J., Henry, M., Tilmes, S., MacMartin, D. G., Kravitz, B., Doherty, S. J., Moore, J., Lennard, C., et al.: G6-1.5 K-SAI: a new Geoengineering Model Intercomparison Project (GeoMIP) experiment integrating recent advances in solar radiation modification studies, Geoscientific Model Development, 17, 2583–2596, https://doi.org/10.5194/gmd-17-2583-2024, 2024.

Visioni, D., Robock, A., Duffey, A., Henry, M., Hirasawa, H., Lee, W. R., Wang, C., Roberts, K., Watanabe, S., Reboita, M. S., et al.: The Geoengineering Model Intercomparison Project (GeoMIP) contribution to CMIP7–description of new experimental protocols and preliminary results, Geoscientific Model Development, 19, 8469–8499, https://doi.org/10.5194/gmd-19-8469-2026, 2026.

Wang, B., ed.: The Asian Monsoon, Springer Praxis Books, Springer, Berlin, Heidelberg, ISBN 978-3-540-37722-1, https://doi.org/10.1007/3-540-37722-0, 2006.

Wang, B. and LinHo, X.: Rainy season of the Asian–Pacific summer monsoon, Journal of Climate, 15, 386–398, https://doi.org/10.1175/1520-0442(2002)015<0386:RSOTAP>2.0.CO;2, 2002.

Wang, B., Yim, S.-Y., Lee, J.-Y., Liu, J., and Ha, K.-J.: Future change of Asian-Australian monsoon under RCP 4.5 anthropogenic warming scenario, Climate dynamics, 42, 83–100, https://doi.org/10.1007/s00382-013-1769-x, 2014.

Wang, B., Jin, C., and Liu, J.: Understanding future change of global monsoons projected by CMIP6 models, Journal of Climate, 33, 6471–6489, https://doi.org/10.1175/JCLI-D-19-0993.1, 2020.

Wang, C.: Uncertainty in Regional Monsoon Responses to Solar Radiation Modification Is Often Greater Across Models Than Across Strategies, Zenodo [Dataset], https://doi.org/10.5281/zenodo.23889423, 2026.

Wang, C., Donner, L. J., and Mahfouz, N. G.: Wind-Driven Circulation Feedbacks Offset Tropical Geoengineered Sea Salt Emissions, Journal of Geophysical Research: Atmospheres, 131, e2026JD047 411, https://doi.org/10.1029/2026JD047411, 2026a.

Wang, C., Visioni, D., Lee, W. R., Duffey, A., Wentland, C. R., Wheeler, L., Wagman, B., Turbeville, S., Watanabe, S., and Henry, M.: Quantifying the effectiveness of multiple SAI strategies across different dimensions, Earth's Future, 14, e2026EF008 696, https://doi.org/10.1029/2026EF008696, 2026b.

Webster, P. J., Magana, V. O., Palmer, T., Shukla, J., Tomas, R., Yanai, M., and Yasunari, T.: Monsoons: Processes, predictability, and the prospects for prediction, Journal of Geophysical Research: Oceans, 103, 14 451–14 510, https://doi.org/10.1029/97JC02719, 1998.

Wilcox, L. J., Liu, Z., Samset, B. H., Hawkins, E., Lund, M. T., Nordling, K., Undorf, S., Bollasina, M., Ekman, A. M., Krishnan, S., et al.: Accelerated increases in global and Asian summer monsoon precipitation from future aerosol reductions, Atmospheric Chemistry and Physics Discussions, 2020, 1–30, https://doi.org/10.5194/acp-20-11955-2020, 2020.

Ye, J. and Wang, Z.: An origin of North American monsoon retreat biases in climate models, Journal of Climate, 36, 4665–4676, https://doi.org/10.1175/JCLI-D-22-0592.1, 2023.

Zhang, R.: Global summer monsoon rainy seasons, International Journal of Climatology, https://doi.org/10.1002/joc.1659, 2008.

https://doi.org/10.5194/egusphere-2026-6788
Preprint. Discussion started: 17 November 2026
© Author(s) 2026. CC BY 4.0 License.



795 Zhang, S., Lu, M., Wright, J. S., and Li, S.: A new lens on South China Sea summer monsoon onset and variability, Geophysical Research Letters, 52, e2025GL118 131, https://doi.org/10.1029/2025GL118131, 2025.